AB-INITIO STUDY OF SUPERIONIC CONDUCTORS

MARZIA BATOOL

DEPARTMENT OF PHYSICS

KINNAIRD COLLEGE FOR WOMEN,

LAHORE, PAKISTAN

2023

AB-INITIO STUDY OF SUPERIONIC CONDUCTORS

A RESEARCH REPORT SUBMITTED TO

KINNAIRD COLLEGE FOR WOMEN

IN FULFILLMENT OF THE REQUIREMENTS

FOR THE DEGREE OF

BACHELORS OF SCIENCE

IN

PHYSICS

BY

MARZIA BATOOL

DEPARTMENT OF PHYSICS

KINNAIRD COLLEGE FOR WOMEN, LAHORE

2023

RESEARCH COMPLETION CERTIFICATE

It is certified that **Ms. Marzia Batool** of BS (session 2019-2023), Department of Physics has carried out research work entitled **"AB-INITIO STUDY OF SUPERIONIC CONDUCTORS"** under my supervision.

It is assured that research work is original and has not yet been published anywhere else.

Supervisor:

_____ Dated: 17-05-2023

Dr. Faiza Uzma

Assistant Professor of Physics

Kinnaird College for Women, Lahore.

_____

Ayesha Aftab

Head of Physics Department

Kinnaird College for Women, Lahore.

"All changes suggested by examiners during defense are incorporated in this final copy."

Student	Supervisor	Head of Department

ANTI-PLAGIARISM DECLARATION

I certify that this is my own research work. The work has not, in whole or in part, been presented elsewhere for assessment. Where material has been used from other sources, it has been properly acknowledged. The similarity index of the research report is **15%**. If this statement is untrue and I am found guilty of plagiarism, the punitive action against me should be taken as per Kinnaird Anti Plagiarism Policy.

Marzia Batool

Registration No: F19BPHY006

Program: BS Physics

Signature:

Supervisor:

_____

Dr. Faiza Uzma

Assistant Professor of Physics

Kinnaird College for Women, Lahore.

_____

Ayesha Aftab

Head of Department:
Kinnaird College for Women, Lahore.

ACKNOWLEDGEMENTS

First and foremost, I would like to praise ALLAH the Almighty, the most Beneficient, Glorious, Omniscient, Gracious and Merciful, who created ua in Muslim Ummah. I greatly thankful to ALLAH for giving me wisdom, strength, courage, and the ability to bar the circumstances throughout the course of my study.

All respect and praise to the Holy Prophet Hazrat Muhammad (P.B.U.H), who came as alight of knowledge for all seekers and a real role model for all mankind.

I feel highly privileged to take this opportunity to express my sincere and deep sense of indebtedness from the core of my heart to my parents who supported me all the way morally and financially, they encouraged me throughout my life and always stand by my side. Without their support it is impossible for me to do all this. I would like to thank my parents from the core of my heart for their love and prayers that have always been a source of courage and confidence for me and key to my success.

I would like to thank my supervisor Dr. Faiza Uzma, whose expertise was invaluable in formulating the research report. Her insightful feedback pushed me to sharpen my thinking and brought my work to the higher level. I am thankful for her patience, inspiring guidance, co-operation throughout my research work, and keen interest as well as the editorial corrections that she made during thesis writing.

May Allah bless all of us. Ameen

Marzia Batool

ABSTRACT

The use of halide materials as solid electrolytes has recently attained gigantic research interest due to their ability to operate at high temperature. Under over present knowledge novel halide electrolytes, such as $LiYCl_4$, $LiSmCl_4$, and $LiAlCl_4$, exhibit high Li-ionic conductivities, approaching 10^{-3} S/cm, with low activation energies. A considerable experimental as well as theoretical efforts have been made in the identification of optimal combination of Li-M-X, (M: metal, X: halide) that are suitable at high temperature. Whereas, being a novel promising electrolyte material, $LiAlCl_4$, there are not too many literatures available for the electronic, structural characteristics analysis of $LiAlCl_4$. However, these characteristics decides the suitable battery material such as the materials with wide bandgap of ~ 6 eV are highly desirable. In this work, we employ Density Functional Theory (DFT) simulations to conduct a study of Li-M-X with M= Al and X =Cl. Electronic, structural properties and phase stability of $LiAlCl_4$ is found. The values of the bandgap 5.63 eV and 5.2 eV are calculated by the exchange correlation functionals, Generalized Gradient Approximation (GGA) with Perdew-Burke-Ernzerhof (PBE) and the Local Density Approximation (LDA) for $LiAlCl_4$, respectively. Results indicate that the GGA-PBE calculation gives a more desirable value closer to the experimental band gap. These results agree with the true nature of GGA-PBE method. On the other hand, experimental synthesis of electrolytes is time-consuming and requires a lengthy process to achieve a perfect solid electrolyte. Computational modeling minimizes cost, time and complements experiments by providing unique theoretical insights to predict the state-of-the-art solid-state electrolytes, which have been rarely reported. Our calculations determined that $LiAlCl_4$ shows promising potential as a battery electrolyte with a band gap of 5.63 eV, indicating the suitability of $LiAlCl_4$ as a superionic conductor.

AB-INITIO STUDY OF SUPERIONIC CONDUCTORS

TABLE OF CONTENTS

LIST OF FIGURES

LIST OF TABLES

LIST OF ABBREVIATIONS

Uninterrupted Power Supplies	UPS
Hybrid Electric Vehicles	HEV
Lithium	Li
Aluminium	Al
Solid-Sate Electrolyte	SSE
Lithium-Ion	Li-ion
Na super-ionic conductor	NASICON
Lithium-Cobalt Oxide	$LiCoO_2$.
Cadmium	Cd
Electrical energy storage	EES
Solid-State Battery	SSB
Li-rich anti-perovskite	Li_3OCl
Lithium Tetrahaloaluminates	$LiAlX_4$
Density Functional Theory	DFT
Tetrahaloaluminates	$LiAlBr_4$
Solid Electrolyte	SE
Ab Initio Molecular Dynamics	AIMD
Exchange-Correlation	XC

Local Density Approximation	LDA
Generalized Gradient Approximation	GGA
Hybrid functional	HF
Orthogonalized Plane Wave	OPW
Ultra-Soft Pseudopotentials	USPP
Norm-conserving pseudopotentials	NCPP
Projected Augmented Waves	PAW
Pseudopotential	PP
Self-Consistent Field	SCF
Visualization for Electronic Structural Analysis	VESTA
Cambridge Serial Total Energy Package	CASTEP
Full Potential Linear Augmented Plane	FPLAP

CHAPTER 1

INTRODUCTION

1.1 Introduction to Batteries

A battery is a device that converts chemical energy to electrical energy battery's chemical reactions involve the flow of electrons from one material (electrode) to another via an external circuit. The flow of electrons generates an electric current, which can be used to perform work. Charged ions flow through an electrolyte solution that is in contact with both electrodes to balance the flow of electrons. Different electrodes and electrolytes cause different chemical reactions, which affect how the battery works, how much energy it can store, and how much voltage it can produce. Alessandro Volta, an Italian Physicist, invented the first battery in 1800 [1].

The following characteristics must be present in a practical battery:

i. It should be light in weight and small in size.
ii. The cell or battery must be capable of providing a constant voltage. Furthermore, the voltage of the battery or cell must not change while in use.

1.1.1 Cell and Battery

Even though the term battery is often used, the basic electrochemical unit responsible for the actual storage of energy is called a Cell. A Cell, as just mentioned, is the fundamental electrochemical unit that is the source of electrical energy produced by conversion of chemical energy. In its basic form, a cell typically contains three main components: two electrodes and electrolyte and also

consists of terminals, separator and a container. Speaking of electrodes, there are two types of electrodes called the Anode (-) and the Cathode (+) [2].

The Anode is the negative electrode (also called the Fuel Electrode or the Reducing Electrode). It loses electrons to the external circuit and in the electrochemical reaction, it gets oxidized. Cathode on the other hand, is the positive electrode (also called the Oxidizing Electrode). It accepts electrons from the internal circuit and in the electrochemical reaction, it gets reduced. Hence, the energy conversion in a battery is due to electrochemical oxidation-reduction reaction [2].

The third important component of a cell is the electrolyte. An electrolyte acts as medium for transfer of charge in the form of ions between the two electrodes. Hence, the electrolyte is sometime referred to as Ionic Conductor. A separator which electrically isolates the positive and negative electrodes. An important point to be noted here that the electrolyte is not electrically conductive but just have ionic conductivity [2].

A battery often consists of one or more "cells" that are electrically connected in either a series or parallel configuration to provide the necessary voltage and current levels [2].

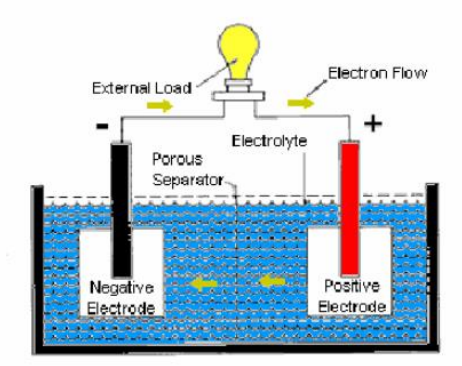

Figure 1.1 Schematic view of Basic Battery with electrochemical cell [3].

1.2 Types of Batteries

Basically, all the electrochemical cells and batteries are classified into two types:

- Primary (non-rechargeable)
- Secondary (rechargeable)

Even though there are several other classifications within these two types of batteries, these two are the basic types. Simply speaking, Primary Batteries are non-rechargeable batteries i.e., they cannot be recharged electrically while the Secondary Batteries are rechargeable batteries i.e., they can be recharged electrically [2].

1.3 Primary Batteries

A Primary Battery is one of the simple and convenient sources of power for several portable electronic and electrical devices like lights, cameras, watches, toys, radios etc. As they cannot be recharged electrically, they are of "use it and when discharged, discard it" type [2].

Usually, primary batteries are inexpensive, light weight, small and very convenient to use with relatively no or less maintenance. Majority of the primary batteries that are used in domestic applications are single cell type and usually come in cylindrical configuration (although, it is very easy to produce them in different shapes and sizes) [2].

1.3.1 Common Primary Battery Types

There are Two Main Types of Primary Cells/Batteries:

1. Alkaline Batteries

Chemical composition of Zinc with Manganese dioxide forms these batteries. The electrolyte that is used in these types of batteries is potassium hydroxide, and since all the contents are purely alkaline, it is termed as an alkaline battery.

2. Coin Cell Batteries

The coin cell batteries also have alkaline electrolytes, and additionally, they also have the chemicals of lithium and silver oxides. These types of primary batteries are highly efficient in ensuring stable and steady voltage [2].

1.4 Secondary Batteries

A Secondary Battery is also called as Rechargeable Battery as they can be electrically recharged after discharge. The chemical status of the electrochemical cells can be "recharged" to their original status by passing a current through the cells in the opposite direction of their discharge [2].

Basically, secondary batteries can be used in two ways:

- In the first category of applications, the secondary batteries are essentially used as energy storage devices where they are electrically connected to a main energy source and also charged by it and also supplying energy when required. Examples of such applications are Hybrid Electric Vehicles (HEV), Uninterrupted Power Supplies (UPS), etc.
- The second category of applications of secondary batteries are those applications where the battery is used and discharged as a primary battery. Once it is completely discharged (or almost completely discharged), instead of discarding it, the battery is recharged with an appropriate charging mechanism. Examples of such applications are all the modern portable electronics like mobiles, laptops, electric vehicles, etc.

Energy Density of secondary batterie are relatively lower than that of primary batteries but have other good characteristics like high power density, flat discharge curves, high discharge rate, low temperature performance [2].

1.4.1 Common Secondary Battery Types

Two of the oldest batteries are in fact secondary batteries called the Lead – Acid Batteries, which were developed in late 1850's and Nickel – Cadmium Batteries, which were developed in early 1900's. Until recent times, there are only two types of secondary batteries [2].

The first and the most commonly used rechargeable batteries are called Lead – Acid Batteries. The second type of the rechargeable batteries are called Nickel – Cadmium Batteries. In the recent decades, two new types of rechargeable batteries have emerged. They are the Nickel – Metal Hydride Battery and the Lithium – Ion Battery. Of these two, the lithium – ion battery came out to be a game changer and became commercially superior with its high specific energy and energy density figures (150 Wh / kg and 400 Wh / L) [2].

1.5 Lithium-Ion Battery

A lithium-ion battery or Li-ion battery is a type of rechargeable battery composed of cells in which lithium ions move from the negative electrode through an electrolyte to the positive electrode during discharge and back when charging [4].

1.5.1 Applications of Li-Ion Battery

Some of the most common applications of lithium-ion batteries are:

- Power backups/UPS
- Mobile, Laptops, and other commonly used consumer electronic goods
- Electric mobility
- Energy Storage Systems

1.5.2 Advantages of Li-Ion Battery

- High Energy Density
- Easy maintenance
- Continuous voltage
- Low Self Discharge
- No requirement for priming
- Variety of models available

1.5.3 Disadvantages of Li-Ion Battery

- Requires higher protection (Inflammable)

- Expensive Sensitive to high temperatures

- Transportation problems

1.6 Background of Lithium-Ion Batteries

For many years, the only suitable battery for portable equipment, such as mobile computing and wireless communications was nickel-cadmium. Pioneer work on the lithium battery began in 1912; however, it wasn't until the 1970s when the first non-rechargeable lithium batteries became commercially accessible. During the oil crisis of the 1970s, an English chemist named Stanley Whittingham began working on the concept of a new battery that was able to recharge on its own in a timely manner. He hoped that this could lead to fossil fuelfree energy in the future. Whittingham attempted to use lithium metal and titanium disulfide as the electrodes, however this caused the batteries to short circuit and catch fire, raising safety concerns about the experiment. In the 1980s, John Goodenough decided to experiment using lithium cobalt oxide as the cathode, doubling the energy potential. This led Akira Yoshino to experiment with using a carbonaceous material, petroleum coke, which led to the finding that the battery was significantly safer without lithium metal. This was the beginning of lithium ion battery development. In the 1990s, lithium ion technology began to gain customer acceptance, causing it to become the battery with the fastest-growing popularity. Lithium battery development was first explored because of the safety concerns of lithium metal batteries. Despite being slightly lower in energy density than lithium metal, lithium ion is extremely safe when charged and discharged following specified safety precautions [4].

1.7 Working of Li-ion Batteries

A lithium-ion (Li-ion) battery is an advanced battery technology that uses lithium ions as a key component of its electrochemistry. During a discharge cycle, lithium atoms in the anode are ionized and separated from their electrons. The lithium ions move from the anode and pass through the electrolyte until they reach the cathode, where they recombine with their electrons and electrically neutralize. The lithium ions are small enough to be able to move through a micro-permeable separator between the anode and cathode. In part because of lithium's small size (third only to hydrogen and helium), Li-ion batteries are capable of having a very high voltage and charge storage per unit mass and unit volume. Li-ion batteries can use a number of different materials as electrodes. The most common combination is that of lithium cobalt oxide (cathode) and graphite (anode), which is most commonly found in portable electronic devices such as cellphones and laptops. Other cathode materials include lithium manganese oxide (used in hybrid electric and electric automobiles) and lithium iron phosphate. Li-ion batteries typically use ether (a class of organic compounds) as an electrolyte [5].

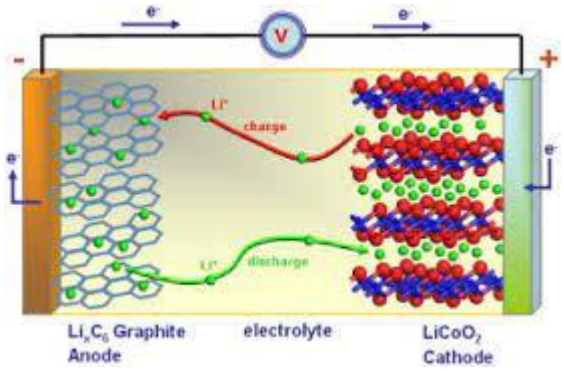

Figure 1.2 Schematic view of the mostly common used Li battery with $LiCoO_2$ as a cathode and graphite anode [6].

1.7.1 Chemistry Involved in Lithium-Ion Batteries

Inside a lithium-ion battery, oxidation-reduction (Redox) reactions take place.

Reduction takes place at the cathode. There, cobalt oxide combines with lithium ions to form lithium-cobalt oxide (LiCoO2). The half-reaction is:

$CoO_2 + Li^+ + e^- \rightarrow LiCoO_2$

Oxidation takes place at the anode. There, the graphite intercalation compound LiC_6 forms graphite (C_6) and lithium ions. The half-reaction is:

$LiC_6 \rightarrow 6C + Li^+ + e^-$

Here is the full reaction (left to right = discharging, right to left = charging):

$LiC_6 + CoO_2 \rightleftarrows 6C + LiCoO_2$

1.8 Solid Electrolytes

A **solid-state electrolyte** (SSE) is a solid ionic conductor and electron-insulating material and it is the characteristic component of the solid-state battery. It is useful for applications in electrical energy storage (EES) in substitution of the liquid electrolytes found in particular in lithium-ion battery. The main advantages are the absolute safety, no issues of leakages of toxic organic solvents, low flammability, non-volatility, mechanical and thermal stability, easy processability, low self-discharge, higher achievable power density and cyclability [7,8].

Solid electrolytes conduct lithium ions at room temperature and can potentially replace conventional organic electrolytes, which are flammable and toxic. In addition to drastically improving the safety of the battery, solid state electrolytes allow the use of

lithium metal as the anode. This in turn increases the cell voltage and thereby increases the energy density of the battery. [9]

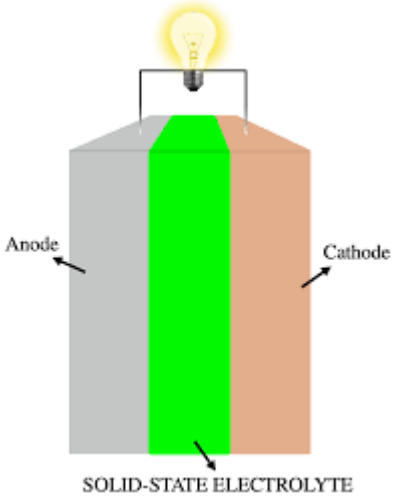

Figure 1.3 All-Solid-State Battery with the solid-state electrolyte [10].

1.8.1 History of Solid Electrolytes

The history of solid-state ionic conductors started with the discovery of conduction property in heated solid Ag_2S and PbF_2 made by Faraday in 1830 [11]. Then a series of electrical conductivity in solid electrolyte is started from 1854-1960 in which stabilized zirconia and silver exhibit high ionic conductivity, which is considered as a turning point for high conductivity in solid electrolytes [12]. In late 1970, the discovery and development of lithium insertion type cathode materials, rechargeable SSBs were introduced. In the 1980s and 1990s, high Li-ion conductivity compounds with high ionic conductivity are attracting more and more research focus on its potential applications in the energy sector storage and conversion equipment, some solid ions conductors were reported during this period. In 1976, the Na super-ionic conductor (NASICON) structure [13] was first designed, in 1993 perovskite [14], in 2003 garnet type important oxide SSE, and finally in 2007 $Li_7La_3Zr_5O_{12}$ [15]

become famous after the report of fast ionic conductivity. In 2011-2016, sulfide SSE like $Li_{10}GeP_2S_{12}$ [16], $Li_7P_3S_{11}$ [17], $Li_{9.54}Si_{1.74}P_{1.44}S_{11.7}Cl_{0.3}$ [18] were found with even higher conductivity (10^{-25} mS/cm) than conventional liquid electrolytes. Another oxide type Li-rich anti-perovskite Li_3OCl [19] was also discovered with high ionic conductivity. In 2019, halide based solid electrolytes have gained significant interest due to their wide electrochemical window (≈ 4 V) and high ionic conductivity (≥10^{-3} S/cm), a detail comparison of sulfides, oxide and halide is given in the Figure 1.4.

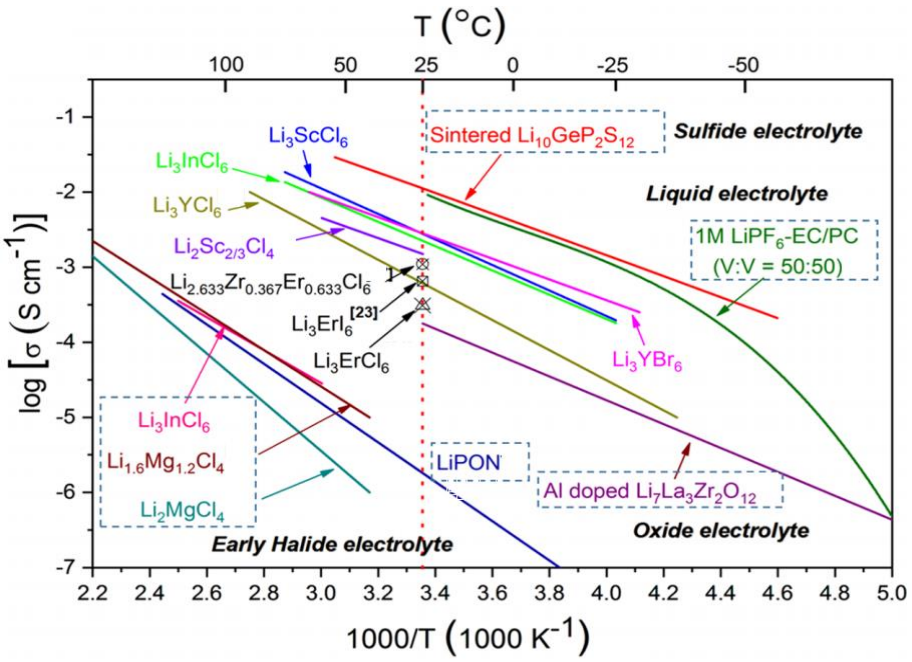

Figure 1.4 Evolution of ionic conductivity of oxide, sulfide and the typical metal halide super-ionic conductors along with organic liquid electrolytes as a function of temperature [20].

1.9 Significance

Generally, for a very fast super-ionic conductors, a structure may compose of crystalline framework of immobile and mobile ions sub-lattice sites, available adjacent

sites must be larger or equivalent to number of mobile species and that mobile ions diffuse from excited sites to neighboring sites with low barrier energy to form a collective and continuous diffusion path. Solid electrolytes of Li have distinct concern from the apprehensive determinations in search of solid electrolytes of various structural forms which is another critical factor for designing a superionic conductor is based on the coordination environment of lithium. The coordination of Li is directly related to ion migration and activation, because the unfavorable coordination of the mobile ion could be extremely feasible for high mobility and low activation energy, however there may difficulty in synthesis due to thermal instability. So, it is a need to explore such type of solid electrolytes which contains intrinsic vacancies and week bonding environment to enhance ionic conductivity [21].

So far, the Li_3MCl_6 family (M = Sc, Y, In, Yb, Er, etc.) is the most successful class of halide superionic conductors. Up till now the main research focus of halide solid electrolytes was remain in finding or discovering new structures with different compositions based on ionic conductivity and stability window voltage (Figure 1.5). However, there are very few research reports that have explored the several issues especially chemical stability of halide for technological, practical and large production for all-solid-state batteries [22].

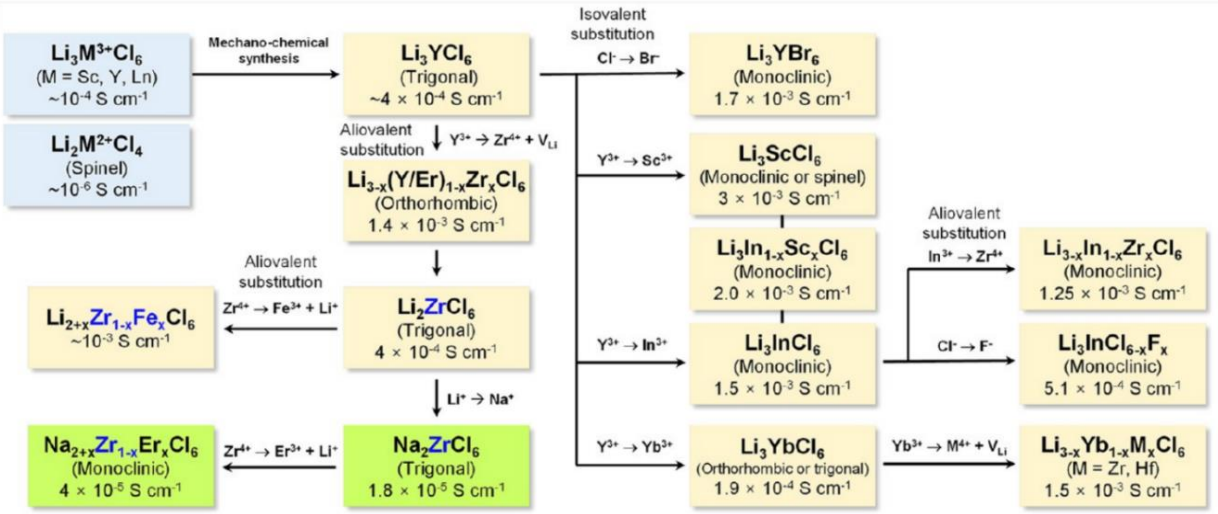

Figure 1.5 Progress and development in exploring halide electrolytes with different composition and structures with their ionic conductivity [23].

It is fact that oxides are compatible with Li metal anode with less ionic conductivity and sulfides with high ionic conductivity but incompatible due to chemical instability, and halides have high ionic conductivity with large electrochemical stability window but are not stable with Li metal anode.

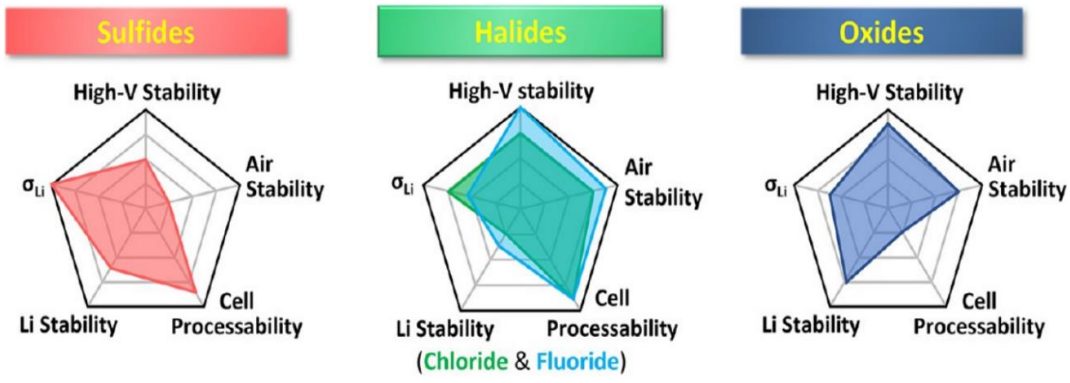

Figure 1.6 Comparison of key performance and properties of sulfides, halides and oxides [23].

It can be seen in Figure 1.6 that oxide and sulfides could meet only two/three out of five key performances of solid electrolytes whereas halides four out five key properties. If the halides become stable with Li metal anode it would open new era for next generation all-solid-state batteries, which is a main objective of this project.

1.10 Halide Electrolytes

Recently, halides based solid electrolytes are attracting significant interest due to high their ionic conductivity ($\geq 10^{-3}$ S/cm) and wide electrochemical window ($\approx$ 4 V) [24]. In fact oxides and sulfides are the most studied electrolytes materials and are among the most promising candidates for solid-state electrolytes in secondary batteries, however oxide material exhibit low Li ion conductivity while sulfides showed narrow electrochemical stability window voltage and incompatibility with Li metal anode [25].Similarly another family of halide based solid electrolytes, Lithium Tetrahaloaluminates, $LiAlX_4$ (X = Cl, Br, I) reported by Nicolás Flores-González et al.by mechanical synthesis for the first time with a space group of monoclinic $P_{21/c}$, Z = 4; a = 8.0846(1) Å; b = 7.4369(1) Å; c = 14.8890(2) Å; β = 93.0457(8)°) [26]. LiAlBr4 exhibited the highest ionic conductivity at room temperature (0.033 mS/cm), while $LiAlCl_4$ showed a conductivity of 0.17 mS/cm at 333 K, coupled with the highest thermal and oxidative stability. Modeling of the diffusion pathways suggests that the Li-ion transport mechanism in each tetrahaloaluminate is closely related and mediated by both halide polarizability and concerted complex anion motions [26].

1.11 Crystal structure of $LiAlCl_4$

$LiAlCl_4$ crystallizes in the monoclinic $P2_1/c$ space group. Li^{1+} is bonded to six Cl^{1-} atoms to form $LiCl_6$ octahedra that share corners with two equivalent $LiCl_6$ octahedra, corners with two equivalent $AlCl_4$ tetrahedra, an edge with one $LiCl_6$ octahedra, and

edges with two equivalent $AlCl_4$ tetrahedra. The corner-sharing octahedral tilt angles are 49°. There is a spread of Li–Cl bond distances ranging from 2.45–2.78 Å. Al^{3+} is bonded to four Cl^{1-} atoms to form $AlCl_4$ tetrahedra that share corners with two equivalent $LiCl_6$ octahedra and edges with two equivalent $LiCl_6$ octahedra. The corner-sharing octahedral tilt angles range from 58–59°. There is a spread of Al–Cl bond distances ranging from 2.13–2.16 Å. There are four inequivalent Cl^{1-} sites. In the first Cl^{1-} site, Cl^{1-} is bonded in an L-shaped geometry to one Li^{1+} and one Al^{3+} atom. In the second Cl^{1-} site, Cl^{1-} is bonded in a 3-coordinate geometry to two equivalent Li^{1+} and one Al^{3+} atom. In the third Cl^{1-} site, Cl^{1-} is bonded in a 3-coordinate geometry to two equivalent Li^{1+} and one Al^{3+} atom. In the fourth Cl^{1-} site, Cl^{1-} is bonded in a bent 120 degrees geometry to one Li^{1+} and one Al^{3+} atom [26].

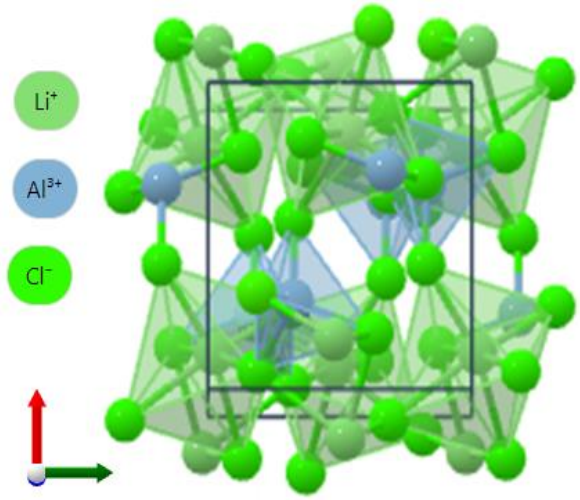

Figure 1.7 Crystal Structure of $LiAlCl_4$ [26].

RATIONALE

In recent times, there has been a wide research interest in the use of halide materials as solid electrolytes, and several new types of halide electrolytes, including Li_3YCl_6, Li_3InCl_6, $Li_2Sc_{2/3}Cl_4$ halo spinel structure, and $LiAlCl_4$, have been synthesized and studied. These electrolytes have exhibited high Li-ionic conductivities even at high temperature, typically around 10^{-3} S/cm, and low activation energies. Solid electrolyte materials based on halides have attracted significant attention due to their wide electrochemical window of approximately ≥4 V. While much research has focused on finding the optimal combination of Li−M−X, which refers to the combination of lithium, metal, and halide ions, little computational attention has been paid to the impact of electronic and structural factors as well as phase stability of novel Li-M-X. To address this gap, this study employs density functional theory (DFT) to predict the structural and electronic properties of the promising material $LiAlCl_4$ as a solid electrolyte for Li-ion batteries. The material $LiAlCl_4$ is particularly promising due to its band gap and a wide electrochemical stability window, both of which reach beyond 4.26 V with respect to Li/Li^+. These properties make $LiAlCl_4$ a potential superionic conductor in solid-state batteries, and a promising candidate for practical applications. Therefore, the electronic, structural and phase stability analyis of such solid electrolyte materials is crucial for the advancement of safe and high-performance solid-state batteries**.**

OBJECTIVES

The study will study one of the promising battery materials that has recentally raised an enormous research interest i.e. Li-M-X. As a prototype we will be working with M = Al and X= Cl_4. The objectives of study are:

- Structure forming on Vesta and Geometry optimization of $LiAlCl_4$ in CASTEP
- Structural parameter calculations for $LiAlCl_4$
  - Lattice constants calculations with different exchange correlation functionals (GGA/LDA) and find the best ones and validate our results with the present literature review for the above-mentioned battery material.
- Electronic properties simulation for $LiAlCl_4$ and check the agreement of these with the present experimental as well as theoretical literature present.
  - Band gap calculations with (LDA/GGA)
  - Total Density of States for $LiAlCl_4$ (LDA/GGA)
  - Partial Density of states for Li, Al and Cl as well as on orbitals s, p and d.
- Phase stability of $LiAlCl_4$

CHAPTER 2

LITERATURE REVIEW

Akihiro Sakai et al. (2018) investigated solid-electrolyte materials based on lithium halides, namely Li_3YCl_6 and Li_3YBr_6, have been discovered to possess crucial properties necessary for all-solid-state battery (ASSB) applications, especially for large-scale implementation. These properties include high lithium-ion conductivity, excellent deformability, and strong chemical as well as electrochemical stability. The cold-pressed powders of these materials exhibit lithium-ion conductivities exceeding 1 mS cm^{-1} at room temperature, without the need for any additional intragrain or grain boundary resistances. When used in bulk-type ASSB cells with $LiCoO_2$ as the cathode material, these halide solid electrolytes display coulombic efficiencies as high as 94%, without any additional coating. The exceptional electrochemical characteristics and material stability of these lithium halide salts indicate that they hold great potential as a candidate for solid electrolytes in ASSB, alongside sulfides or oxides [24].

Shuo Wang et al. (2019) studied solid electrolytes with high Li-ion conductivity and electrochemical stability are necessary to enable all-solid-state Li-ion batteries. Recent experimental findings have identified Li_3YCl_6 and Li_3YBr_6 as potential new solid electrolytes. Using first principles computation, they investigated the Li-ion diffusion, electrochemical stability, in addition to that, interface stability of chloride and bromide materials, whereas identified the reasons behind their high ionic conductivities along with good electrochemical stabilities. Unlike sulfide and oxide Li-ion conductors, chloride and bromide chemistries have low migration energy barriers, wide electrochemical windows, that are not restricted by previous design principles, allowing for greater flexibility in developing fast Li-ion conductors. This study

emphasizes chloride and bromide as a promising new avenue for research on solid electrolytes with high ionic conductivity as well as good stability [27].

Fiaz Hussain et al. (2019) investigated the role of solid electrolytes in modern electrochemical energy storage technologies is significant, but achieving high Li-ion conductivity in them is still a major challenge. A recent study reports an improvement in ion conductivity in the anti-spinel structure of Li_3OBr, which was synthesized recently, due to the presence of intrinsic vacancies. The anti-spinel Li_3OBr has a stable defective structure with a high concentration of octahedral vacancies, leading to exceptionally high Li mobility (0.136 mS cm^{-1} at room temperature) as confirmed by ab initio molecular dynamic simulations. This mechanism of ion conductivity enhancement through octahedral vacancies in anti-spinel Li_3OBr represents a new approach to solid electrolyte material design [28].

Roman Schlem et al. (2020) investigated due to their high ionic conductivity and good oxidation stability, halide-based solid electrolytes are becoming more popular for use in solid-state batteries. While their stability at the cathode interface is well-established, their stability against the lithium metal anode has been explored. This study examines the reaction layer formed between Li_3InCl_6 (Li_3YCl_6) and lithium using sputter deposition of lithium metal, as well as in-situ X-ray photoelectron spectroscopy and impedance spectroscopy. The results indicate that the interface is thermodynamically unstable and leads to a continuously growing interphase resistance. In addition, impedance spectroscopy was used to examine the interface between Li_3InCl_6 and Li_6PS_5Cl, to determine whether combining them as cathode electrolyte and separator electrolyte could result in stable, low impedance operation over the long term. While halide-based lithium superionic conductors are not suitable for use against Li due to oxidation instability, they show promise as cathode electrolytes [29].

Jianwen Liang et al. (2021) studied solid-state electrolytes (SSEs) are crucial materials for the development of rechargeable all-solid-state Li batteries (ASSLBs), which are

the upcoming generation of electrochemical energy storage systems. The discovery of new superionic conductors is an ongoing area of research, with various types of SSEs having been developed so far, including polymer-, oxide-, and sulfide-based SSEs. Recently, metal-halide SSEs (Li-M-X, where M is a metal element and X is a halogen) have emerged as new candidates due to their numerous advantageous properties, including wide electrochemical stability windows (0.36–6.71 V vs Li/Li^+) and better chemical stability towards cathode materials compared to other SSEs. Additionally, some metal-halide SSEs (such as Li_3InCl_6 developed by their group) can be synthesized at large scales in a water solvent, without requiring special apparatus or handling in an inert atmosphere. This article focuses on the topic of metal-halide SSEs and aims to provide guidance for further development of novel halide SSEs to meet the multiple requirements of energy storage devices [30].

Nicolás Flores-González et al. (2021) studied advanced oxides and sulfides, that possess excellent lithium-ion conductivity and electrochemical stability. They highly promising materials for solid-state electrolytes in secondary batteries. However, newly emerging halides are showing potential as alternatives due to their intrinsic low energy barriers for lithium-ion migration, high oxidative stability, and favorable mechanical properties. Through mechanochemical synthesis, the characterization of $LiAlX_4$ compounds has been expanded, and the synthesis of $LiAlI_4$ in a monoclinic P21/c crystal structure with Z = 4, and dimensions of a = 8.0846(1) Å, b = 7.4369(1) Å, c = 14.8890(2) Å, and β = 93.0457(8)° has been achieved for the first time. Among the tetrahaloaluminates, $LiAlBr_4$ demonstrated the highest ionic conductivity at room temperature (0.033 mS cm^{-1}), while $LiAlCl_4$ exhibited a conductivity of 0.17 mS cm^{-1} at 333 K, along with the highest thermal and oxidative stability. Diffusion pathway modeling suggests that the transport mechanism of lithium ions in each tetrahaloaluminate is closely related and is mediated by both halide polarizability and concerted complex anion motions [26].

Kwangnam Kim et al. (2021) studied that despite exploring various solid electrolyte (SE) options, it has been difficult to achieve the desired combination of stability, performance, and processability. Recently, lithium ternary halides have been gaining attention for SEs due to their high ionic conductivity and wide electrochemical window. This research aims to develop a material design strategy for lithium halides Li_3MX_6 (where X is Cl, Br, or I) for use in high-voltage all-solid-state Li-ion batteries. This is achieved through the systematic investigation of crystal structures, phase and electrochemical stabilities, electronic and mechanical properties, and ionic conductivities. The results of calculations show that the electronegativity difference between M and X affects structural properties and stabilities. Monoclinic phases are preferred due to weak Coulomb interactions in Li_3MX_6. Moreover, the oxidation potential and chemical stability against cathode materials of Li_3MX_6 are better for smaller X, with chlorides exhibiting the highest oxidation potential (∼4.3 V) among Li_3MX_6. This makes chlorides an appropriate choice for SEs for high-voltage cathodes. The band gap and elastic moduli increase for relatively small X, suggesting that chlorides have low electronic conductivity and elastic deformability. Chlorides with transition metals typically exhibit trigonal phases, wider electrochemical stability windows, larger band gaps, and higher elastic moduli than other types of halides. Additionally, chloride Li3MCl6 is expected to have high ionic conductivities with the aliovalent substitution of M^{3+} to Zr^{4+} and the anion mixing of Cl with Br. This study provides fundamental guidelines for the development of lithium halide SEs for high-voltage all-solid-state Li-ion batteries [31].

Fiaz Hussain et al. (2022) investigated solid electrolytes made of halide materials have recently gained moderate attention in research. Several new halide electrolytes, including Li_3YCl_6, Li_3InCl_6, and $Li_2Sc_{2/3}Cl_4$ halospinel structure, and $LiAlCl_4$, have been experimentally prepared, and they show high Li-ionic conductivities close to 10^{-3} S/cm with low activation energies. However, while much experimental and theoretical work has focused on finding the best combination of Li−M−X, less attention has been

given to understanding the effects of the structural characteristics on the ionic conductivities and electrochemical stabilities. To address this, the authors conducted a comparative study using DFT and AIMD simulations on several halide electrolytes with different structures, such as rock-salt Li_3MCl_6, spinel $Li_2Sc_{2/3}Cl_4$, and $LiMCl_4$. Their results reveal that halospinel $Li_2Sc_{2/3}Cl_4$ structures with cubic symmetry exhibit exceptional three-dimensional conductivity and mechanical stability as superionic conductors, with Li-ionic conductivity ranging from 0.26−19.0 mS/cm and activation energy lower than 0.20 eV (0.342−0.195 eV). Among them, $Li_2Sc_{2/3}Cl_4$ is predicted to have the best balance between ionic conductivity and stability, with a room-temperature ionic conductivity as high as 15.3 mS/cm and a band gap and electrochemical stability window vs Li/Li^+ reaching 4.26 V, respectively. Therefore, this material shows great promise for practical applications as a superionic conductor in solid-state batteries [32].

Hiram Kwak et al. (2022) studied halide superionic conductors have emerged as a promising alternative to sulfide or oxide solid electrolyte (SE) materials for all-solid-state batteries (ASSBs) due to their favorable properties, such as high Li^+ conductivity, good chemical and electrochemical oxidation stabilities, and mechanical deformability. In this article, recent advancements in Li^+- and Na^+-conducting SEs using halide materials are comprehensively summarized. The article starts by introducing the ionic diffusion mechanism and the factors that govern crystal structures. It then discusses design strategies, including substitution and synthesis protocols, to further enhance the properties of halide materials. Theoretical and experimental results on electrochemical stabilities and compatibilities with electrode materials are also reviewed. Additionally, challenges and issues associated with developing practical ASSB applications are discussed, such as cost considerations, stabilities in atmospheric air, aqueous solutions, and slurry-processing, and the fabrication of sheet-type electrodes (or SE membranes) for large-format ASSBs. Finally, the article offers a perspective on future research directions for halide SEs, emphasizing the need to expand the materials space [23].

Fiaz Hussain et al. (2023) studied the demand for low-cost, environmentally friendly, and renewable energy from next-generation all-solid-state batteries is growing rapidly. All-solid-state sodium-ion batteries (ASSSIBs) are considered superior to all-solid-state lithium-ion batteries due to their superior environmental properties, higher safety, and increased availability on Earth. However, the development of ASSSIBs requires solid-state sodium electrolytes that possess certain characteristics such as high ionic conductivity at room temperature, wide electrochemical stability window, low electronic conductivity, and compatibility with interfaces, which have been rarely reported. To address this challenge, the authors used density functional theory and ab initio molecular dynamic simulations to predict novel sodium solid electrolytes. Their research resulted in the discovery of several sodium superionic conductors with excellent ion-conducting properties and interface compatibility. The optimized composition they found exhibited a remarkable Na-ionic conductivity of up to 8 mS cm^{-1} and an extremely low activation energy of 0.20 eV, in addition to high chemical and electrochemical stabilities. This discovery has the potential to be a focal point for future experimental studies and accelerate the development of high-performance ASSSIBs [33].

Han-xin Mei et al. (2023) compared to conventional lithium-ion batteries, solid-state batteries (SSBs) possess higher safety and energy density, making the solid-state electrolyte (SSE) a critical component that has garnered significant attention. SSEs are typically categorized into three types: oxides, sulfides, and polymers. This article focuses on the latest research on unconventional solid-state electrolytes (USSEs), including halides, zeolites, and others, discussing their properties, structures, synthesis methods, and costs. While halides are less popular, they are gaining popularity due to their many benefits, such as ionic conductivity at room temperature of over 0.6 mS cm^{-1}, higher stability than most SSEs, even with an oxidation potential above 4V, ease of handling in dry air, and the feasibility of mass production using liquid phase methods. The article also compares typical USSEs to conventional SSEs, such as

oxides and liquid electrolytes, in various aspects. Finally, the article concludes with future research directions for USSEs, as well as practical application challenges that need to be addressed [34].

Kaiyong Tuo et al. (2023) conducted research on rechargeable solid-state batteries (ASSBs) that utilize solid-state electrolytes (SSEs) are seen as the next generation of devices for storing electrochemical energy. Among the many important research areas in energy storage chemistry, the development of SSEs is particularly crucial. Recently, halide SSEs have been the focus of intensive research for use in ASSBs because of their excellent combination of high ionic conductivity, chemical and electrochemical stability, and mechanical deformability. This review provides a critical overview of the synthesis, chemical stability, and outstanding challenges of halide SSEs. It summarizes in detail the design strategies, such as element substitution and crystal structure design, that have been utilized to optimize the ionic conductivity of halide SSEs. The review also discusses issues related to solvent compatibility, humid air stability, and degradation mechanisms associated with halide SSEs. Additionally, the review highlights advanced in situ/operando characterization techniques applied to halide-based ASSBs. It provides a comprehensive understanding of interface issues, cost issues, and scalable processing challenges related to halide-based ASSBs for practical applications. Finally, the review presents future perspectives on designing high-performance electrode/electrolyte materials that can guide the development of halide-based ASSBs for energy storage and conversion [35].

CHAPTER 3

MATERIALS AND METHODS

3.1 Historical Background

According to the Heisenberg uncertainty principle, position and momentum cannot be measured simultaneously for a particle. Classical mechanics insufficiency in describing the nature of the material at the Nano-scale led to the foundation of quantum physics. Theoretically, we have to use quantum chemistry approximations to understand the interactions within the molecule and its environment. These approximations almost replicate the physical behavior of atoms and electrons as they interact with their nuclei. History has witnessed a glorious evolution of quantum chemical methods [36]. This chapter briefly summarizes the basics of ab-initio approximation methods starting from Born-Oppenheimer approximation to multiconfigurational methods.

The basic quantum mechanical many-body Schrödinger wave equation, $\hat{H}\Psi = E\Psi$, under some boundary conditions, can be obtained by substituting momentum function with the position derivative ($p_x \rightarrow d/dx$). Here, $\hat{H}$ and Ψ is the system's Hamiltonian and many-electron wavefunction, simultaneously. The wavefunction of 'n' number of nuclei and electrons is given by,

$$\hat{H}\Psi\,(x_1, x_2, \ldots, x_n, R_1, R_2, \ldots, R_n) = E\Psi(x_1, x_2, \ldots, x_n, R_1, R_2, \ldots, R_n) \quad (3.1)$$

Where x_n is the electronic spin and space position and R_n is nucleic vice versa. However, to make it solvable the continuum nature of the equation had to be made discrete [37].

3.2 Born-Oppenheimer Approximations

Born interpreted that the wave function itself is not an observable but it is only a probability amplitude. Whereas its square gives us a statistical concept of intrinsic properties of the material such as position. By momentum substitution, for the interaction within the atom, the time-independent Schrödinger wave equation's Hamiltonian becomes,

$$\hat{H} = \sum_{i>j}^{N} \frac{1}{r_{ij}} - \sum_{i=1}^{N} \frac{\nabla_i^2}{2} - \sum_{A=1}^{M} \frac{\nabla_A^2}{2M_A} - \sum_{A=1}^{M} \sum_{i=1}^{N} \frac{Z_A}{r_{iA}} \sum_{A>B}^{M} \frac{Z_A Z_B}{R_{AB}} \quad (3.2)$$

The Hamiltonian is known as Born-Oppenheimer Hamiltonian, where $\nabla^2 i$ is Laplacian or kinetic energy. *i* and *j* are accounted for electrons and A and B on the nuclei. Born-Oppenheimer approximation simplifies this complicated expression. For any fixed molecular geometry, the electrons surrounding nuclei are lighter in weight and they will take effect from the heavy nuclei [38].

If the kinetic energy is coming from nuclei, then the third term in the above equation 3.2 will be neglected. Though to recover energy difference the nuclei-nuclei repulsion contribution can be added at the end of all electronic calculations [38].

$$\hat{H} = \sum_{>j}^{N} \frac{1}{r_{ij}} - \sum_{i=1}^{N} \frac{\nabla_i^2}{2} - \sum_{A=1}^{M} \sum_{i=1}^{N} \frac{Z_A}{r_{iA}} \sum_{A>B}^{M} \frac{Z_A Z_B}{R_{AB}} \quad (3.3)$$

To analytically solve this equation is a cumbersome task, therefore, computational scientists tried to find some approximate solutions to make it solvable on the computer. The wave equation can be solved by applying the adiabatic approximations. The approximation methods are generally divided into two groups, ones that incorporate electron-interaction such as DFT and others that explicitly incorporate or don't incorporate electron correlation such as tight-binding or Hartree approximation [39].

3.3 Theory of Electron

The discovery of electron put a great challenge for theoretical physics to describe the theory of electron in condensed matter. The theory of electron in condensed matter is a

many-body problem in which statistical concepts are used to describe the intrinsic properties of materials in a large system. The theory requires approximations, in which each electron moves independently with others at some average effective potential. With the passage of time and development of electron theory, a critical step was to understand the band theory of independent electrons in crystals [40].

3.4 Hartree-Fock Approximation

After the development of quantum mechanics, Thomas and Fermi established an approximation in 1927 for calculating the kinetic energy for the electron system and distribution in heavy atoms in which the electrons are surrounded by the nucleus without considering exchange and correlation. [41,42] Dirac developed the local approximation for exchange later in 1930 [43]. Eventually, by the middle of the 1960s, computers acquired enough memory and processing power to solve the Schrödinger's wave equation for atoms and tiny molecules using the Hartree-Fock approximation. This method accounts for the classical electrostatic potential for other electron-electron interactions as well as non-local exchange interactions and involves all electrons interacting with the fixed nuclei's external potential. The many electron wavefunction in stationary condition can be roughly approximated using this variational method. A Slater determinant can approximate wavefunction for N electrons system or N spin-orbitals [44].

Wavefunction for single electron is written by

$$\Psi (r_1, r_2 \dots r_n) = \varphi_1 (r_1)\, \varphi_2 (r_2) \dots \varphi_n (r_n) \qquad (3.4)$$

For the two-electron system it can be written as

$$\Psi = \varphi_a (1)\, \varphi_2 (2) \qquad (3.5)$$

Anti-symmetry principle by a wavefunction,

$$\Psi_A = 1/\sqrt{2}\, [\varphi_a (1)\, \varphi_b (2) - \varphi_a (2)\, \varphi_b (1)] \qquad (3.6)$$

Hartree-Fock Solution (Fock, Slater in 1930)

Slater determinant (SD)

$$\Psi_{SD}(r_1, r_2, \dots, r_n) = \frac{1}{\sqrt{N!}} \begin{vmatrix} \varphi_1(1) & \varphi_2(1) & \cdots & \varphi_N(1) \\ \varphi_1(2) & \varphi_2(2) & \cdots & \varphi_N(2) \\ \vdots & \vdots & & \vdots \\ \varphi_1(N) & \varphi_2(N) & \cdots & \varphi_N(N) \end{vmatrix} = |\varphi_1, \varphi_2 \cdots \varphi_N\rangle \quad (3.7)$$

3.5 Density Functional Theory and mathematical formulism

Schrodinger equation can be solved easily for one electron system. For multiple electronic system, it is very hard to solve Schrodinger equation, because we have to solve for each of the electronic part. So, we introduce some of approximations, one of them is DFT. DFT calculations are like Ab initio and semi empirical calculations, based on Schrodinger equation. However, unlike the other two methods, DFT does not calculate a conventional wave function, but rather derives the electron distribution functional directly. A functional is a mathematical entity related to function. DFT calculations are usually faster than Ab initio, but slower than semi empirical [45].

In DFT the functional is the electron density which is a function of space & time. Electron density is used in DFT as the fundamental property unlike Hartree-Fock theory which deals directly with the many-body wavefunction. Using the electron density significantly speeds up the calculation. Whereas the many-body electronic wavefunction is a function of 3N variables (the coordinates of all N atoms in system) the electron density is only a function of three variables x,y,z [45].

Any property of a system of many interacting particles that described as a functional of ground state density $p(\boldsymbol{r}) = p(x, y, z)$ is called the fundamental principle of density functional theory (DFT), where a functional is just a function that depends on a function [44]. In 1964, P. Hohenberg and W. Kohn formulated the modern density

functional theory based on density as "basic variable" for all properties of the system as a unique functional of the ground state density [46]. In 1965 the formulation of density functional theory presented by the W. Kohn and L. J. Sham become practical, accurate and feasible approach for the many body systems of electrons in atoms, molecules and solids [47]. Though Kohn-Sham equations were able to capture exact kinetic energy of the system completely. Today, DFT has become an upsurge tool for computing electronic structure in condensed matter, quantum states of atoms, molecules, solids and as well as other finite systems, and ab initio molecular dynamics (AIMD) simulations of solids which provides the ground state energy $E[p(\boldsymbol{r})] = E\ [p\ (x, y, z)]$ of system [44,48]. One of the drawbacks of density functional theory is that it cannot consider many-body wavefunction. Whereas Hartree-Fock can by using Slater determinant. In general, DFT can be described by the basic DFT theorems which are also known as Hohenberg and Kohn theorems : [44,46]

3.5.1 Hohenberg-Kohn theorems

The first theorem states that "The external potential V_{ext} $(\boldsymbol{r})$ of any system of interacting particles is uniquely determined by the ground state energy density $p(\boldsymbol{r})$ i.e. the ground state properties of a many-electron system depend only on the electronic density $p(\boldsymbol{r})$." The second theorem states that "a universal functional for the energy $E[p(\boldsymbol{r})]$ assumes its minimum value for the ground state density p_0 $(\boldsymbol{r})$ with respect to all densities fulfilling $\int p(\boldsymbol{r})d(\boldsymbol{r}) = N$, i.e. for any particular $V_{ext}(\boldsymbol{r})$, the exact ground state energy of the system is the global minimum value of this functional, and the density $p(\boldsymbol{r})$ that minimizes the functional is the exact ground state density p_0 $(\boldsymbol{r})$ [44,46].

3.5.2 Kohn-sham energy

After Hohenberg-Kohn found the possibility to describe the quantum system with its corresponding electron density, Kohn and Sham proposed a quick way of calculations without the explicit evaluation of wavefunction for the system. Kohn-Sham assumed

the system of non-interacting electrons under the influence of external potential has a density that matches with the electronic density of its exact counterpart. Consider a system of N interacting electrons in a non-degenerate ground state associated with an effective potential $Vext(\boldsymbol{r})$ [44,46].

$$E[N] = K[N] + \int Vext(\boldsymbol{r})N(\boldsymbol{r})d\boldsymbol{r} + J(r) + Exc[N] \qquad (3.8)$$

Where $K[N]$ is non-interacting kinetic energy, $J(r) = \frac{1}{2}\int\int \frac{N(r)N(r')}{|r-r'|} d\boldsymbol{r}'\, d\boldsymbol{r}$ is classical Coulomb's repulsion of particles charge density. $Vext(\boldsymbol{r})$ is external potential that is, attractive potential due to the presence of positively charged nucleus and $Exc[N]$ is the exchange and correlation term that incorporates all the rest of the interactions in the interacting particles system. Equation 3.8 leads to the famous Kohn-Sham equations [44,46].

3.6 Exchange-Correlation (XC) Potential and Functional

The exchange-correlation functional describes the energy associated with the exchange and correlation interactions between the electrons in a system. The exact form of the exchange-correlation functional is not known, and various approximate forms have been developed and widely used. The most commonly used approximate forms are the local density approximation (LDA) and the generalized gradient approximation (GGA). LDA assumes that the electronic density of a system can be approximated by the electronic density of a homogeneous electrons gas at the same electron density. GGA functional include information about the gradient of the electron density, which is thought to improve the accuracy of the calculation. Hybrid functional are a combination of DFT and wave function theory (HF or DFT) that can be used to improve the accuracy of the calculation. The development of new and more accurate exchange-correlation functionals is an active area of research in DFT [49].

The one electron equation can also be written as

$$\left(-\frac{1}{2}\nabla^2 + V_{eff}(\boldsymbol{r})\right)\psi_k(\boldsymbol{r}) = \varepsilon_k\psi_k(\boldsymbol{r}) \quad (3.9)$$

The term $Veff(\boldsymbol{r})$ is called effective potential that is defined as

$$V_{eff}(\boldsymbol{r}) = V_{ext}(\boldsymbol{r}) + V_{xc}(\boldsymbol{r}) + \int d\boldsymbol{r}' p(\boldsymbol{r}')\frac{1}{|\boldsymbol{r}-\boldsymbol{r}'|} \quad (3.10)$$

So putting the value of effective potential to the above equation (3.9), we get

$$\left(-\frac{1}{2}\nabla^2 + V_{ext}(\boldsymbol{r}) + V_{xc}(\boldsymbol{r}) + \int d\boldsymbol{r}' p(\boldsymbol{r}')\frac{1}{|\boldsymbol{r}-\boldsymbol{r}'|}\right)\psi_k(\boldsymbol{r}) = \varepsilon_k\psi_k(\boldsymbol{r}) \quad (3.11)$$

It leads to

$$E = \sum_{K=1}^{N}\varepsilon_k - \frac{1}{2}\int d\boldsymbol{r}\int d\boldsymbol{r}'\frac{p(r)p(r')}{|r-r'|} + E_{xc}[p] - \int d\boldsymbol{r}V_{xc}[p(\boldsymbol{r})]p(\boldsymbol{r}) \quad (3.12)$$

From the above equation only $E_{xc}[p]$ and $V_{xc}[p(\boldsymbol{r})]$ are approximated, where $V_{xc}[p(\boldsymbol{r})]$ is also known as exchange correlation potential.

In general, $E_{xc}[p]$ and $V_{xc}[p(\boldsymbol{r})]$ can be separated into the exchange ε_x and correlation ε_c parts in terms of energy per particle.

$$E_{xc}[p] = E_x[p] + E_c[p] = \int p(r)\varepsilon_x[p(r)]\,dr + \int p(r)\varepsilon_c[p(r)]\,dr \quad (3.13)$$

The exchange-correlation energy defined as $E_{xc}[p] = T[p] - T_0[p] + U_{xc}[p]$ (3.14)

$T[p] - T_0[p]$ is the difference between the kinetic energy of interacting and non-interacting systems and $U_{xc}[p]$ is the Coulomb inter-action of electrons with exchange correlation. Exchange Correlation energy is mainly contribution from the quantum effects apart from kinetic energy and Coulomb's repulsion. XC energy also known as bonding energy. This correlation energy is little fraction of complete electronic energy but its contribution is significant when the energy differences at atomistic scale are essential. Such as in Born-Oppenheimer potential surface. It is inevitable to model this

XC energy correctly [44,48]. Few of the basic approximations in density functional theory are described below.

3.6.1 Local Density Approximation (LDA)

This approximation is accurate for nearly homogeneous system and for limit of large density. One of LDA's limitations is the inability to estimate band gaps precisely. Considering exchange and correlation energy per electron in a homogeneous gas, devised the approximation known as LDA [50]. Hence, correlation energy is provided by

$$E_{xc} = \int d\boldsymbol{r} p(\boldsymbol{r}) \varepsilon_{xc}(p(\boldsymbol{r})) \qquad (3.15)$$

$\varepsilon_{xc}(n(p))$ is exchange correlation energy of a uniform (homogeneous) electron gas. Forming an energy functional leads to LDA approximation, whereas minimizing this by Kohn-Sham method will give LDA approximation of DFT. Mathematically LDA is defined as

$$E_{xc}^{LDA}[p] = \int d\boldsymbol{r} p(\boldsymbol{r}) \varepsilon_{xc}(p(\boldsymbol{r})) \qquad (3.16)$$

Up to now we assumed that electron gas is unpolarized that is the spin per electron is zero.

The exchange-correlation energy as a functional of spin densities are expressed as local spin density (LSD) approximation as follows

$$E_{XC}^{LSD}[p_\uparrow, p_\downarrow] = \int d^3 r \, p \, \epsilon_{XC}^{unif}(p_\uparrow, p_\downarrow) \qquad (3.17)$$

where = $p\uparrow + p\downarrow$, and $p\uparrow$, $p\downarrow$ are spin density of spin up and spin down electrons respectively [50].

3.6.2 Generalized Gradient Approximation (GGA)

GGA functional is a well-known functional and one of the most widely used functionals. Mathematically it can be written as

$$E_{XC}^{GGA}[p_{\uparrow}, p_{\downarrow}] = \int d^3 r \, f(p_{\uparrow}, p_{\downarrow}, \nabla p_{\uparrow}, \nabla p_{\downarrow}) \quad (3.18)$$

Exchange- correlation as a function of density and its gradient of density is determined numerically, where the exchange- correlation potential is written as

$$V_{xc}[p(\boldsymbol{r})] = \frac{\partial E_{xc}[p]}{\partial n[\boldsymbol{r}]} - \nabla \cdot \frac{\partial E_{xc}[p]}{\partial(\nabla n[\boldsymbol{r}])} \quad (3.19)$$

The GGA for correlation is calculated by the following relation.

$$E_C^{GGA}[p_{\uparrow}, p_{\downarrow}] = \int d^3 r \, p[\boldsymbol{\epsilon}_C^{unif}(r_s, \boldsymbol{\zeta}) + H(r_s, \boldsymbol{\zeta}, t) \quad (3.20)$$

r_s is local Seitz radius (p=3/4 $r = 3/4\pi r^3_s = k^3\mathrm{F}/ 3\pi^{\,2}$), $\boldsymbol{\zeta} = (p\uparrow - p\downarrow)\, p/$ is relative spin polarization, $t = |\nabla n| / 2\emptyset k_s p$, dimensionless density gradient.

The GGA for the exchange energy

$$E_X^{GGA} = \int d^3 r \, p\boldsymbol{\epsilon}_X^{unif}(p) F_X(s) \quad (3.21)$$

where $\boldsymbol{\epsilon}_X{}^{unif} = -\,3e^{\,2}k_F\, 4\pi$

The method of constructing GGA exchange related functional divide into two categories. We can choose any functional form for any purpose, according to a group led by Becke, and the quality of this form is determined by actual calculations [51]. Usually, the parameters of such a functional are obtained by fitting a large amount of calculated Data. On the other hand, Perdew believed that the development of exchange-related functionals must be based on certain physical laws, including scale relations, gradual progress, and so on. A well-known GGA functional constructed based on this concept is the PBE functional and one of the most widely used GGA

functionals [44]. Different LDA schemes are similar, but different GGA schemes may give completely different results.

3.7 Hybrid Functionals

Local density approximation (LDA) and generalized gradient approximations (GGA) are successfully used for the calculations and predictions of many accurate properties like ground state energy in DFT, however the both functionals underestimate the bandgap values due to discontinuity exchange correlation potential as compared to experiment. Several techniques, like as the GW approximation, were put out to deliver precise results, but they are computationally expensive and outside the scope of the DFT [53]. Similar to BLYP (Becke and Lee-Yang-Parr) and HSE (Heyd-Scuseria-Ernzerhof) functionals, a novel idea of a hybrid functional was introduced. For bandgap calculations, HSE is known as a more precise hybrid functional; it is based on the common GGA Perdew-Burke-Ernzerhof functional (GGA-PBE) [52]. The mathematical form of the proposed HSE functional is created by adding exchange energy to the mixed Hartree Fock and PBE exchange energy of the standard GGA-PBE functional. The expression for HSE is as follow [53],

$$E_X^{HSE} = aE_X^{HF,SR}(\mu) + (1-a)E_X^{PBE,SR}(\mu) + E_X^{PBE,LR}(\mu) \quad (3.22)$$

where a represents mixture parameter, μ indicates range of Hartree-Fock correction, $E_X{}^{HF,\,SR}(\mu)$and $E_X{}^{PBE,\,SR}(\mu)$and $E_X{}^{PBE,\,LR}(\mu)$ describe short range Hartree Fock, short range and long range PBE exchange energy respectively. HSE hybrid functional is now widely used to predict band gap in superionic conductors, which then leads to an estimation of the upper limit of electrochemical window [54,55].

3.8 Pseudopotentials

The very large G components describe the region of space where the wavefunction is varying very quickly. This happens when the potential is very attractive – the strongest

potentials are those near the nuclei. The wavefunctions near the nuclei are not actually very interesting, because they don't affect the chemical, mechanical or electronic properties very much. We can replace the Coulomb potential near each nucleus with a modified, weaker potential. This modified potential is called a pseudopotential. Now the wavefunctions don't vary as quickly near the nucleus, so we can use a smaller plane-wave cut-off energy. The core electrons spend all their time near the nucleus. They repel the outer electrons, so the outer electrons feel a weaker potential from the nucleus, but otherwise they don't affect the chemical properties etc. Provided we reproduce this screening effect, we can ignore these core electrons altogether! We consider each atom's nucleus and core electrons as an ion, and produce a pseudopotential that has the same effect on the outer electrons. Not only have pseudopotentials reduced the cut-off energy we need, they've also let us concentrate on the valence electrons, reducing the number of states we need from our Schrödinger equation [56].

All pseudopotential approaches are based on the frozen core approximation. In this approximation the effect of the local chemical environment on core-electrons is assumed to be weak and treated by first order perturbation theory. Therefore, the wave functions of the core-electrons are frozen and equal to those of the isolated atom. Only the valence electron wave functions are updated during the self-consistent iterations. Due to the requirement of orthogonality, valence wave functions have rapid oscillations in the core region of the core wave functions. Outside this core region, the core wave functions are essentially zero, which results in much smoother valence wave functions in this region. To treat the rapid variation of the valence wave functions in the core region a large number of plane waves are needed for convergence. One way of getting around this problem is the use of a pseudopotential, in which the interactions of the valence electrons with the nuclei and the core-electrons are described by an effective, much weaker potential. The resulting pseudo-wave functions are smooth inside the core region and are equal the real wave functions outside the core region. The

number of plane waves required to describe the pseudo-wave functions is much less than for the real wave functions, more. Several different pseudopotentials exist, for example orthogonalized plane wave (OPW), norm-conserving pseudopotentials (NCPP), ultra-soft pseudopotentials (USPP) and the projected augmented waves (PAW) method. The USPP and PAW methods are known to converge with a relatively small number of plane waves. Since the PAW is a more general method compared to USPP [57].

3.9 Energy Cut-off

The cutoff energy tells us about the cutoff on the number of plane wave functions being utilized as basic functions to represent the wavefunction. Theoretically, an infinite number of basic functions is required to produce an exact answer. However, this is not computationally feasible and a cutoff must be [58].

The plane-wave expansion is exact in the limit of infinite number of reciprocal lattice vectors G. In practice only, a limited number of G vectors can be used whose maximum kinetic energy

$$E_{cut} \geq \frac{\hbar^2}{2m}|\mathbf{k}+\mathbf{G}|^2,$$

is increased until convergence of total energies and their derivatives is achieved.

E_{cut} keyword is to set the number of plane waves used to calculate the DFT. If the value is high for the calculation of plane waves, the accuracy of the calculation is improved, but it takes a longer time to calculate it. We always have to ensure the cut-off energy is high enough to give accurate results. We repeat the calculations with higher and higher cut-off energies until the properties we're interested in have converged [59].

To describe the internal electrons localized on atomic cores, a large number of G vectors would be needed. The pseudopotential (PP) technique assumes that the most relevant physical properties of a system, as bonding and chemical reactivity, are

brought about by its valence electrons only, and considers ionic cores as frozen in their atomic configurations. The valence electrons thus move in the effective external field produced by these inert ionic cores whose scattering properties are reproduced by the pseudopotential [60].

3.10 k-point Sampling

The k-point is defined based on the size of the real space cell. For the larger the real space the smaller k-point spacing will be required to sample the Brillion zone. The rule of thumb in this prospect is that if the size of the cell chosen is larger than 16 Å in all the dimensions then single gamma centered k-point sampling is sufficient for the system [61].

k-points are used in two different contexts in the vast majority of cases:

- the sampling of the Brillouin Zone, with the goal to produce integrated quantities (e.g. the charge density, the electronic energy, the electronic DOS) that are numerically precise;
- or the specific computation of wavefunctions and eigen energies e.g. to get an electronic band structure.

3.11 Self-Consistent Field (SCF)

Self-consistent field (SCF) methods include both Hartree-Fock (HF) theory and Kohn-Sham (KS) density functional theory (DFT). Self-consistent field theories only depend on the electronic density matrices predicted, and are the simplest level of quantum chemical models [62].

3.12 Theoretical Methods (DFT and AIMD simulations)

Many key characteristics of alkali ion batteries can be accurately by these methods such as ionic transport mechanism and stability by DFT and AIMD simulations. The performance of any alkali-ion battery (electrolytes and electrodes) is judged by some

important characteristics and properties. An electrolyte could be an ideal for commercial and technological applications for batteries if it is thermodynamically, mechanically, energetically and electrochemically stable with electrodes and exhibit good ionic conductivity. The mentioned properties of electrolyte are discussed below.

3.12.1 Phase Stability

In general phase stability of a material is calculated by constructing phase diagram. Phase diagram is constructed by computing the Gibbs free energy of all possible phases belonging to given chemical system at 0 K by performing spin polarization calculations [63] Gibbs free energy can be calculated as

$$G = H - TS = E + PV - TS \quad (1)$$

Where G is Gibbs free energy, H stands for enthalpy, T and S stands for temperature and entropy of the system, E represents internal energy, P and V are pressure and volume of the system. If the hull energy is 0 the system is known as stable system and if hull energy is positive the system is known as unstable/meta-stable depending on the amount of hull energy.

3.12.2 Electrochemical Stability

The performance of solid electrolyte could be estimated by their electrochemical window voltage with electrodes. The electrochemical window can be examined with two thermodynamics approximations [63]. In first approximation Na is assumed as mobile species. In this condition Na act as an open system for the electrolyte and electrode interface. Base on this approach lithium grand potential phase diagram is constructed at different lithium potentials by the following reaction.

$$\emptyset = E - \mu_{Na} N_{Na} \quad (2)$$

where E, $\mu_{Na}$and N_{Na} are the internal energy, Na chemical potential and number of Na atoms in the open system respectively. The phase equilibria of grand Na chemical potential are evaluated for a system at high voltage $\mu_{Na} \approx \mu_{Na}^{0}$ as anode interface and

at low voltage $\mu_{Na} \approx \mu_{Na}^{0} - 5eV$ as cathode interface. The grand sodium chemical potential phase diagrams provide information about the solid electrolyte either they are stable against Na metal anode or undergoes reduction or uptake Na at low voltage or electrolyte oxidized and lost Na at high voltage.

3.13 Flowchart of Theoretical Method (DFT)

Theoretical method for DFT can be seen in the Figure 3.1 below.

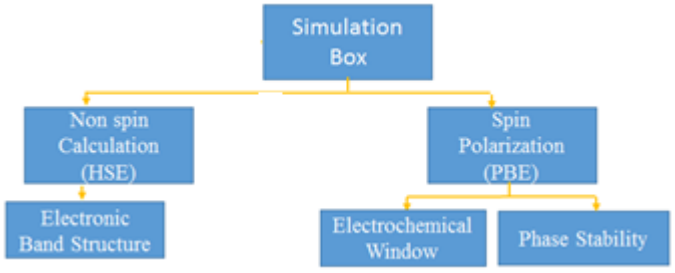

Figure 3.1 Schematic diagram for performing computational using DFT [63].

3.14 VESTA

VESTA (short for Visualization for Electronic Structural Analysis) is a 3D visualization program for structural models, volumetric data such as electron/nuclear densities, and crystal morphologies. VESTA software simulates structures that are more precise and have intermediate responsiveness. VESTA software is a viable option because it is potable and publicly available. It is simply to use and may create stunning crystal structures. Dr Ruben A. Dilanian and Dr. Fuijo Izumi created VESTA. he software allows you to deal with a virtually unlimited number of objects such as atoms, bonds polyhedral, and polygons on iso-surfaces in multiple windows, each of which may contain multiple tabs corresponding to files. VESTA enables you to visualize interatomic distances and bond angles that are restrained in Rietveld analysis with

RIETAN-FP and supports lattice transformation from conventional to non-conventional lattice by using matrices. Other features include the ability to run arithmetic operations among multiple volumetric data files and to export high-resolution graphic images which incorporate smooth rendering of iso-surfaces and sections [64].

3.15 Construction of Structure of $LiAlCl_4$

3.15.1 Main Window

The first is to open a page at VESTA is known as Main Window as shown in Figure 3.2.

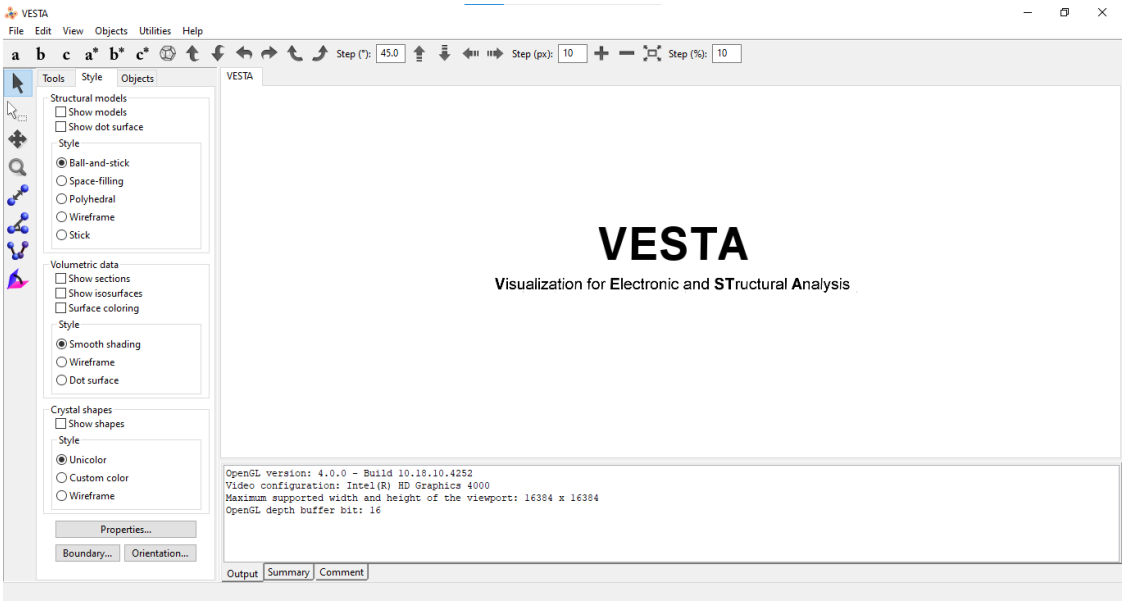

Figure 3.2 Main Window of VESTA.

3.15.2 Unit Cell

Next step in order to construct crystal structure of $LiAlCl_4$ click on ‘edit’ from top bar of main window and then click on ‘unit cell’ from the menu bar as shown in Figure 3.3.

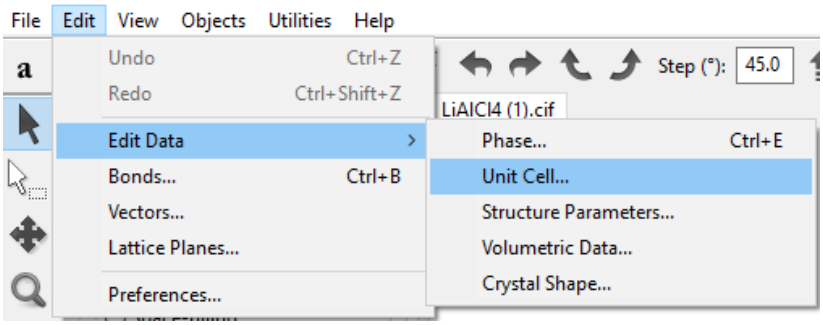

Figure 3.3 Selecting unit cell for construction of crystal structure.

3.15.3 Selecting Parameters

Selecting parameters for monoclinic Lithium Tetra chloroaluminate $LiAlCl_4$ in 3-dimensions for making a cubic crystal structure. After clicking on 'unit cell' in next step another window will appear where we can select their symmetry and lattice parameters for construction of $LiAlCl_4$ as shown in Figure 3.4. Type of lattice selected for this is 'P' and space group is 14 P 21/c. Then click on 'Apply' and 'Ok' to execute.

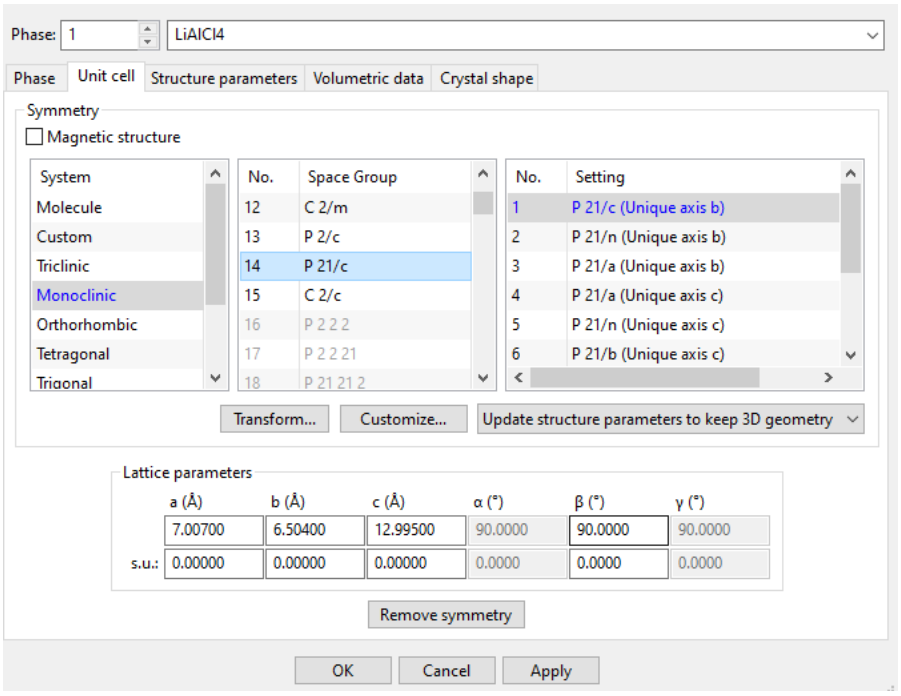

Figure 3.4 Selecting symmetry of unit cell $LiAlCl_4$ [26].

3.15.4 Displaying Structure of $LiAlCl_4$

After clicking on 'structure parameters', in next step another window will appear where we can write their atomic parameters for construction of $LiAlCl_4$ as shown in Figure 3.5. Then click on 'Apply' and 'Ok' to execute. After that complete structure of Lithium tetra chloroaluminate $LiAlCl_4$ will be appear on main window of Vesta as shown in Figure 3.6.

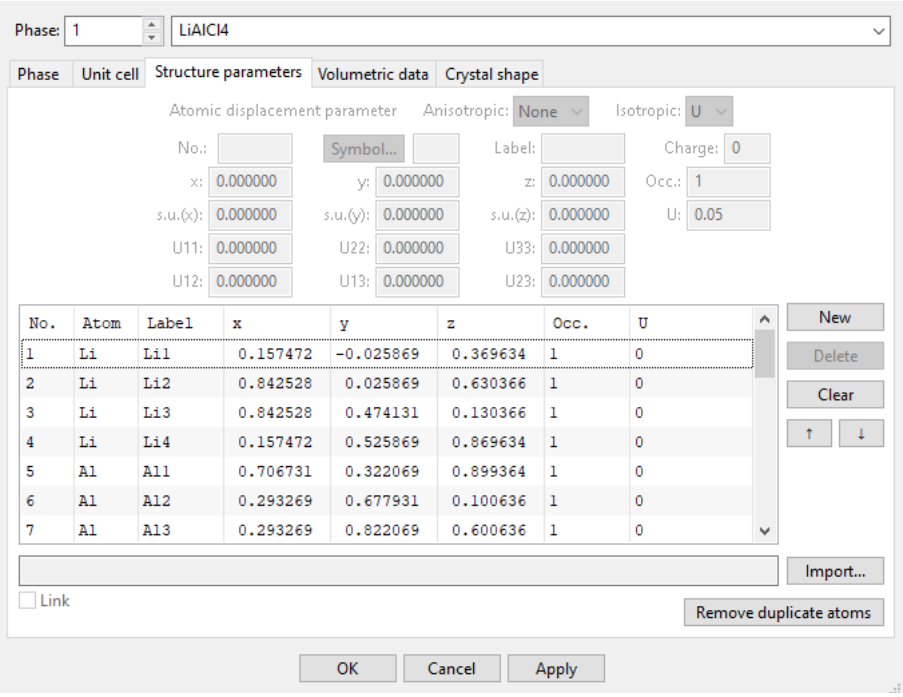

Figure 3.5 Atomic Parameters of $LiAlCl_4$ obtained from Rietveld refinement against SPXD data [26].

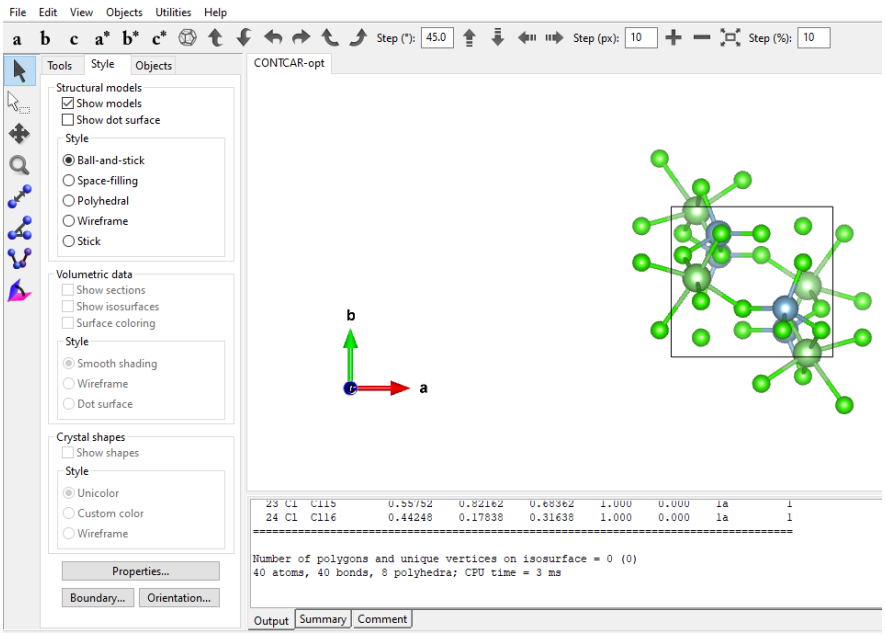

Figure 3.6 Crystal Structure of $LiAlCl_4$

3.16 Description of Crystal Structure of $LiAlCl_4$

$LiAlCl_4$ crystallizes in the monoclinic $P2_1/c$ space group. Li^{1+} is bonded to six Cl^{1-} atoms to form $LiCl_6$ octahedra that share corners with two equivalent $LiCl_6$ octahedra, corners with two equivalent $AlCl_4$ tetrahedra, an edge with one $LiCl_6$ octahedra, and edges with two equivalent $AlCl_4$ tetrahedra. The corner-sharing octahedral tilt angles are 49°. There is a spread of Li–Cl bond distances ranging from 2.45–2.78 Å. Al^{3+} is bonded to four Cl^{1-} atoms to form $AlCl_4$ tetrahedra that share corners with two equivalent $LiCl_6$ octahedra and edges with two equivalent $LiCl_6$ octahedra. The corner-sharing octahedral tilt angles range from 58–59°. There is a spread of Al–Cl bond distances ranging from 2.13–2.16 Å. There are four inequivalent Cl^{1-} sites. In the first Cl^{1-} site, Cl^{1-} is bonded in an L-shaped geometry to one Li^{1+} and one Al^{3+} atom. In the second Cl^{1-} site, Cl^{1-} is bonded in a 3-coordinate geometry to two equivalent Li^{1+} and one Al^{3+} atom. In the third Cl^{1-} site, Cl^{1-} is bonded in a 3-coordinate geometry to two

equivalent Li^{1+} and one Al^{3+} atom. In the fourth Cl^{1-} site, Cl^{1-} is bonded in a bent 120 degrees geometry to one Li^{1+} and one Al^{3+} atom [26].

3.17 MATERIALS STUDIO

BIOVIA Materials Studio is a complete modeling and simulation environment designed to allow researchers in materials science and chemistry to predict and understand the relationships of a material's atomic and molecular structure with its properties and behavior. Using Materials Studio, researchers are engineering better performing materials of all types, including catalysts, polymers, composites, metals, alloys, pharmaceuticals, batteries and more [65]. There are different tools in material studio which are used for computational method and calculations. We have selected CASTEP for geometry optimization, structural parameter calculations and electronic properties simulation for $LiAlCl_4$.

3.17.1 Introduction of CASTEP

It is a quantum mechanics-based program designed for solid-state materials science. CASTEP employs the density functional theory plane-wave pseudopotential method which allows to perform first principle quantum mechanics calculations that explore the properties of crystals and surfaces in materials such as semiconductor, ceramics and metals It involve studies of surface chemistry, structural properties, band structure density of states and optical properties [66].

3.17.2 To select a CASTEP task

- Choose Modules/CASTEP/ calculation from the menu bar to display the CASTEP calculation dialog
- Select the setup tab
- Select the required CASTEP task from the task dropdown list

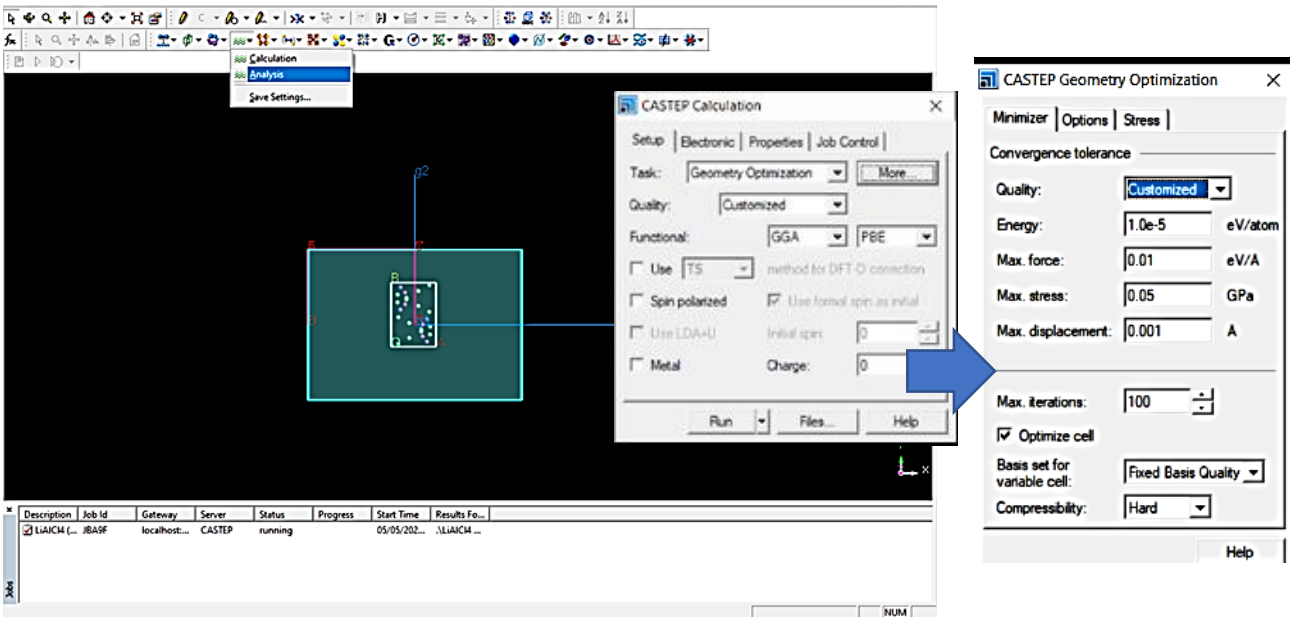

Figure 3.7 Main Window of Material Studio with CASTEP tool calculation for geometry optimization.

3.17.3 Getting started with CASTEP

The basic controls used to define the calculations are available on the set up and electronic tabs of the CASTEP calculation dialog.

We selected geometry optimization task, customized quality and functional are GGA and PBE then apply Run and other window is appeared with the name of CASTEP geometry optimization where values are adjusted for energy, Max force, Max stress and Max displacement as shown in figure 3.7. This method usually provides the fastest way of finding the lowest energy structure and this is the only scheme that supports cell optimization in CASTEP.

The difference between them lie on their treatment of electron exchange correlation effects and the numerical method that they adopt to approximate solution like Full Potential Linear Augmented Plane (FPLAP) wave potential using VASP. Few of the $LiAlCl_4$ explorations has also utilized pseudopotential Cambridge serial Total Energy

Package (CASTEP) and calculated electronic, structural and other properties. Overall, experimental measurements in comparison of mentioned FPLAP pseudopotential for $LiAlCl_4$ crystals showed good agreement in their geometry optimized calculations. This method will be calculated for GGA and same procedure will be adopted for LDA calculations by only changing exchange correlational functional.

3.18 Convergence for Geometry Optimization

The convergence criteria for geometry optimization of $LiAlCl_4$ can depend on the specific computational method and parameters used, as well as the desired accuracy of the results. However, typical convergence criteria for geometry optimization calculations using density functional theory (DFT) may include a maximum force threshold and a maximum displacement threshold.

3.18.1 Steps for convergence geometry optimization of $LiAlCl_4$

Click on the electronic tab on CASTEP calculation window, selects the desired values and functions then open the next tab properties where we selected Band structure, Density of States and Electron Density difference, after that check the settings of job control then apply Run and another window appears with the name of CASTEP Analysis as shown in figure 3.8. By clicking on view bar, the convergence graph for geometry optimization of $LiAlCl_4$ is appeared as shown in below figure 3.8.

LDA Calculations:

Cutoff energy, convergence criteria and all the other convergence parameters are all kept same for LDA exchange correlation functional as they were in the GGA PBE geometry optimization calculations.

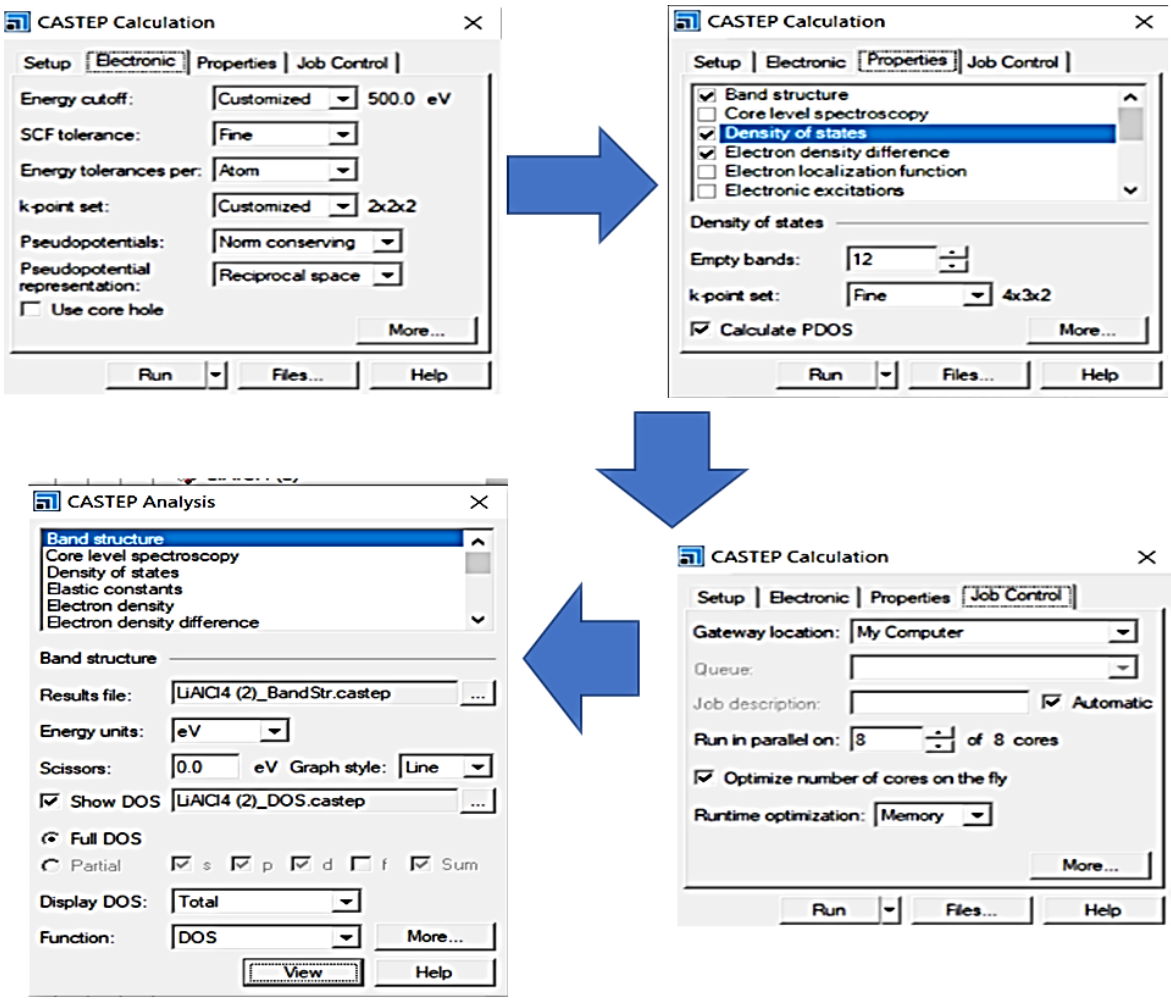

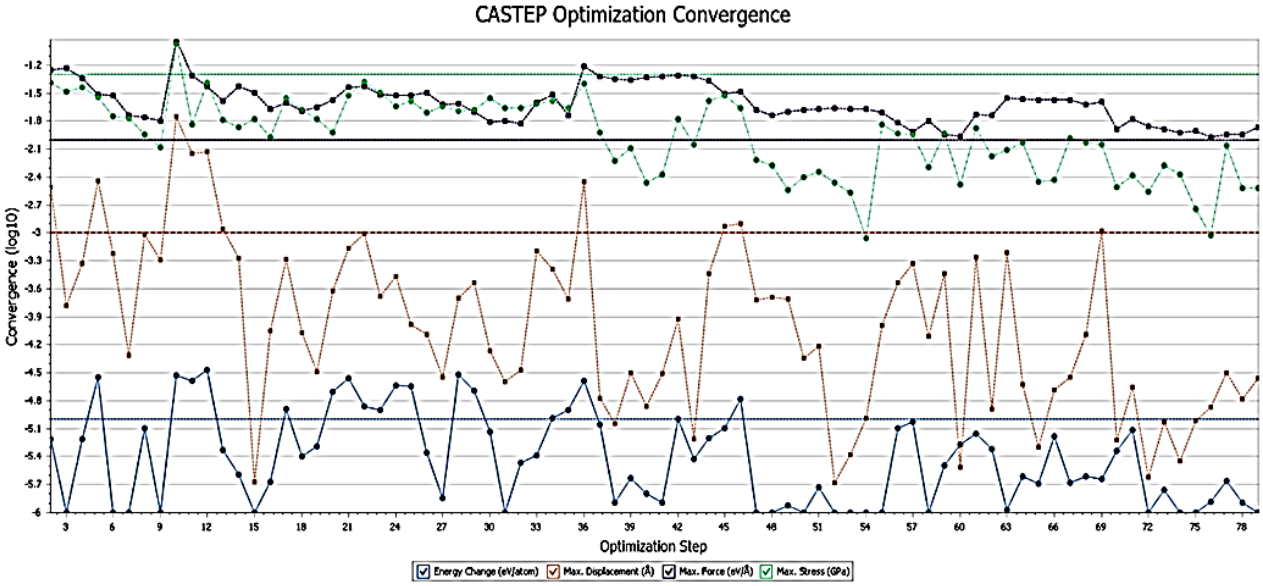

Figure 3.8 Convergence Graph for optimization of structure $LiAlCl_4$.

CHAPTER 4

RESULTS AND DISCUSSION

Atomic configuration are- Li: $1s^2\ 2s^1$,Al: $1s^2\ 2s^2\ 2p^6\ 3s^2\ 3p^1$.and for Cl $1s^2\ 2s^2\ 2p^6\ 3s^2\ 3p^5$.All calculations are carried out on CASTEP which is based on plane wave pseudopotential Method. Initially cutoff energy was optimized on possibly minimum unit cell in crystal lattice at ambient conditions. For optimization cutoff energy is taken 500eV for both GGA and LDA. Points at which both approximations committed approximately no variations in curve are deliberated as reliable and stable. Underneath Bloch theorem, plane wave cutoff energy was diversified till 500 eV with periodicity. At 500 eV of cutoff energy both lattice constants and band gaps become consistent in the two exchange correlations and literature review shows that 500 eV cutoff energy is sufficient [67]. In consequence of this fact, 500 eV of cutoff energy is adopted in all calculations in this study. k-point selection was taken as customized. Monkhorst Pack grid 4×3×2 (customized) is opted on Brillouin zone for electronic calculations. Increase of k points beyond it showed no significant effect, similar was also observed earlier by Z. Usman et al [68]. All analysis were done on primitive cell and later on results were obtained on conventional cell.

4.1 Potential Energy Convergence

To save time we have proceeded step by step first geometry optimization was done for the convergence of Energy. The following figure indicates the final geometry optimization energy convergence curve that was obtained.

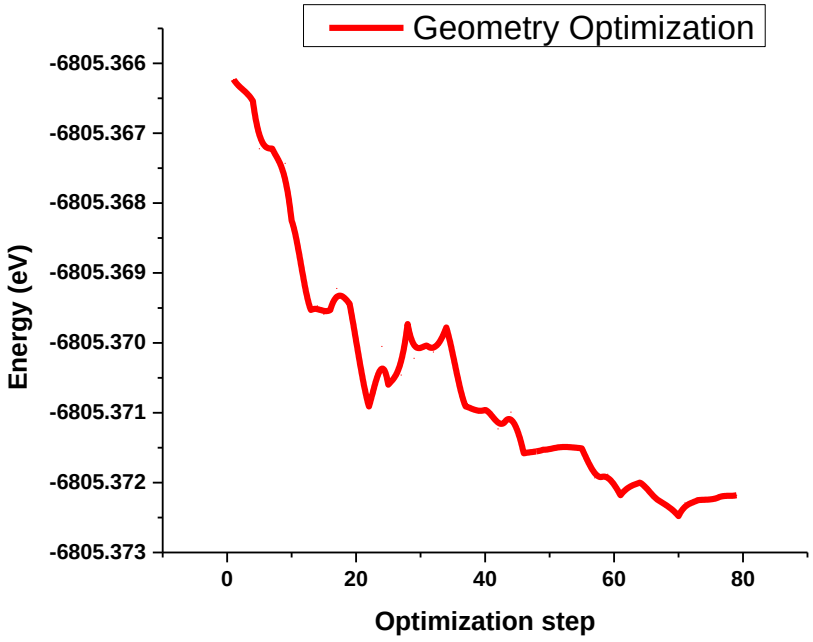

Figure 4.1 Graph for Geometry Optimization of $LiAlCl_4$.

4.2 Geometry optimized structure

After geometry optimization through GGA-PBE the following structure was achieved that was further used for various properties calculations. To check the reliability of this optimized structure we have compared our calculated structural parameters with the available literature present to date under our knowledge. The table shows that our calculated lattice parameters are in good agreement with the present experimental [69,70] and computational [26] study. The percentage error is very low the low percentage error can be attributed to the usage of high convergence criteria such as 10^{-6} eV/atom cut of energy and maximum force of 0.01 eV/angstrom This indicates the good reliability of our structure and that we can further proceed for electronic calculations too.

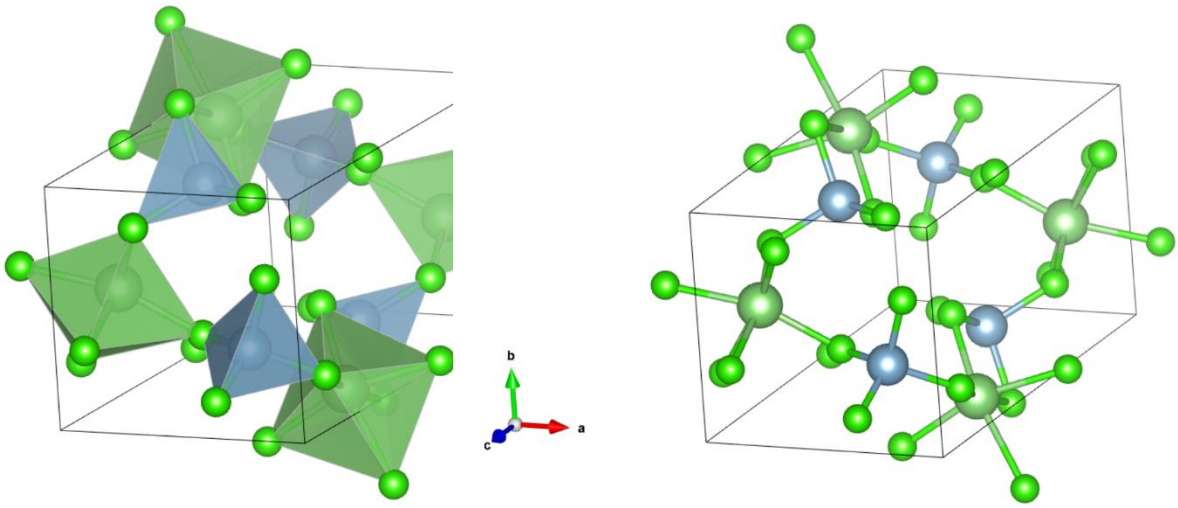

Figure 4.2 Optimized Structure for $LiAlCl_4$.

4.3 Generalized gradient approximation with Perdew Berke (GGA-PBE)

4.3.1 Lattice Parameters

The Lattice parameters found for GGA-PBE are a = 7.14 Å, b= 9.33 Å and c = 13.9 Å Following table indicate that the lattice parameters are reasonably good agreement with present literature.

Table 4.1 Comparison of Bandgap energies and Lattice parameters of various materials.

Material	Structure	Lattice Parameters (Å)	Band gap Energy (eV)
$LiAlCl_4$ (experimental)	Monoclinic	a = 7.0044(1) b = 6.5074(1) c = 12.995(1)	5.56
$LiTa_2PO_8$ (theoretical)	Monoclinic	a = 12.137 b = 12.137	About 5 eV

		c = 8.536	
Li_3PS_4 (experimental)	Argyrodite		
		a = 10.424	Around 3.4eV
		b = 10.553	
		c = 6.125	
$LiYCl_4$ (theoretical)	Monoclinic	a =7.07	
		b =6.57	
		c =13.125	> 6

Note: experimental and theoretical data is collected from ref: [69,26, 70, 71, 72,73].

Current Calculations			
GGA -PBE			
LiAlCl4	**Monoclinic**	**a = 7.14, b= 9.33 and c = 13.9 Å**	
			5.6 eV
LDA			
LiAlCl4	**Monoclinic**	**a = 7.14, b= 9.33 and c = 13.9 Å**	
			5.2 eV

4.3.2 Band Structure

A wide bandgap is found in band structure by GGA-PBE calculations for $LiAlCl_4$ as shown in figure 4.3.

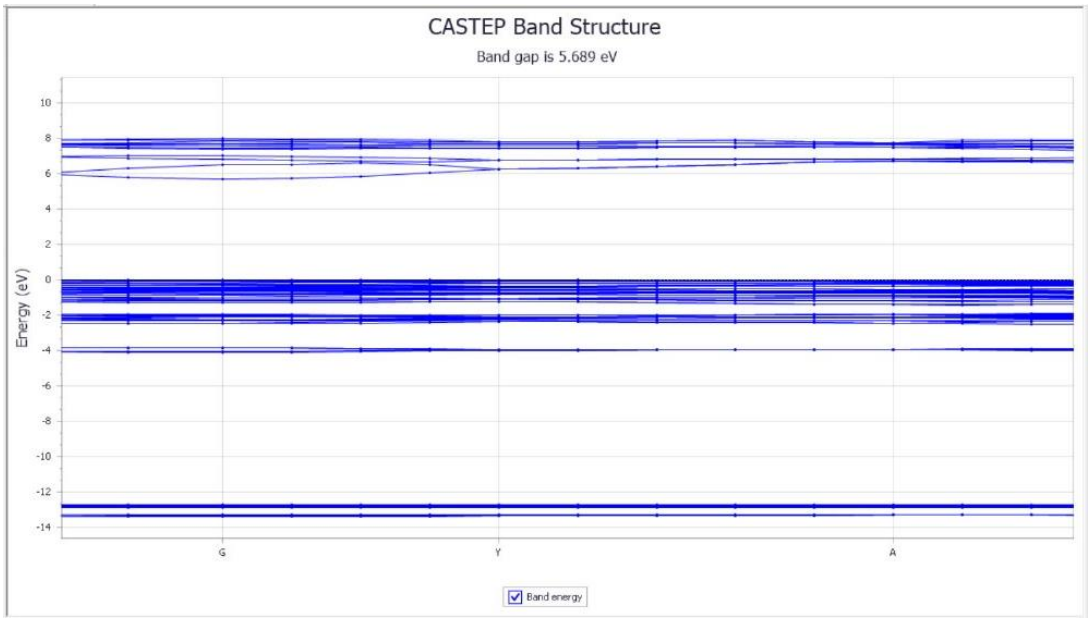

Figure 4.3 Band structure by GGA-PBE calculations for $LiAlCl_4$.

The Bandgap found is 5.63 eV. That is in good agreement with the bandgap described in the literature which is 5.56eV. This value indicate that this material has a very large bandgap that makes it a promising material for battery electrolyte material.

4.4 TDOS and PDOS Calculations for $LiAlCl_4$

Total Density of States (TDOS) and Partial Density of States (PDOS) calculations are commonly used to investigate the electronic properties of materials. In this work, we have performed DFT calculations to calculate the TDOS and PDOS for $LiAlCl_4$ using the GGA-PBE and LDA-PBE exchange-correlation functional. The TDOS plot shows the total number of energy states as a function of energy. The PDOS plot shows the

contribution of each individual atomic orbital to the total DOS. In our calculations, we have considered the contribution of Li, Al, and Cl atoms to the PDOS.

The TDOS plot for $LiAlCl_4$ shows a clear band gap, indicating that the material is an insulator. The valence band (VB) is dominated by the Cl- 3p orbitals, while the conduction band (CB) is mainly composed of the Li^+ 2s and Al 3p orbitals. The energy gap between the VB and CB is about 5.63 eV, which is consistent with the experimental value.

The PDOS plots for Li, Al, and Cl atoms show that the valence states are mainly composed of Cl 3p orbitals, while the conduction states are primarily formed by Li 2s and Al 3p orbitals. The Li 1s and Al 2p orbitals also contribute to the conduction states, but to a lesser extent. These results indicate that the electronic properties of $LiAlCl_4$ are primarily determined by the Cl atoms, while the Li and Al atoms play a secondary role. This indicates that the electronic properties of $LiAlCl_4$ are mainly determined by the Cl^- and Li^+ ions.

The DOS and PDOS calculations reveal that $LiAlCl_4$ is an insulator with a band gap of about 5.63 eV. The Cl- 3p orbitals dominate the valence band, while the Li^+ 2s and Al 3p orbitals contribute to the conduction band. These results provide valuable insights into the electronic properties of $LiAlCl_4$ and can guide the design of novel solid electrolytes for Li-ion batteries.

4.4.1 Partial Density of States (PDOS)

The figure 4.4 shows partial density of states by GGA-PBE calculations for $LiAlCl_4$.

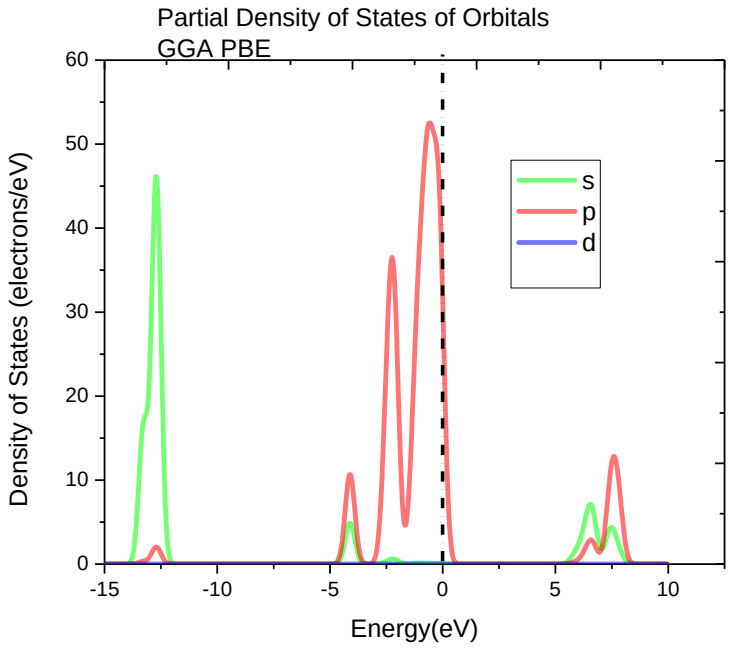

Figure 4.4 Partial density of states versus energy plot of $LiAlCl_4$, calculated using GGA-PBE method.

The above graph indicates the contribution of individual atomic orbitals to the total density of states as a function of energy.

The horizontal axis of the graph represents the energy levels of the material, while the vertical axis represents the density of states. Each line in the graph corresponds to a different atomic orbital, and the contribution of that orbital to the total density of states at each energy level.

The different colors of the lines in the graph represent the different atomic species (Li, Al, and Cl).

The PDOS plot can provide valuable information about the electronic properties of the material, such as the location and width of the band gap, the bonding and hybridization of different atomic orbitals, and the electronic states that are responsible for specific properties, such as ionic conductivity or electrochemical stability.

4.4.2 Total Density of States (TDOS)

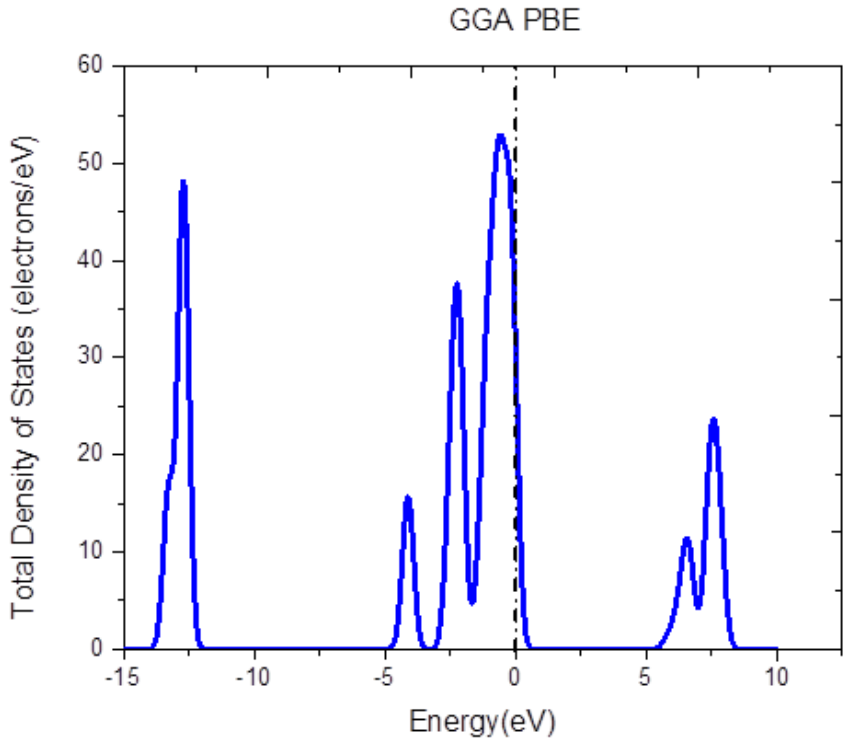

Figure 4.5 Total density of states versus energy plot of $LiAlCl_4$, calculated using GGA-PBE method.

Above graph showing the distribution of electronic states with respect to energy.

The DOS graph indicates that $LiAlCl_4$ is an insulator with a band gap of about 5.63 eV, which is the energy range between the valence band and the conduction band. The valence band is located below the Fermi level (0 eV), and the conduction band is located above it. The Fermi level represents the highest occupied energy level in a material at absolute zero temperature.

4.5 Electron Cloud Isosurface of different elements in $LiAlCl_4$

The isovalue adopted is 0.25 for left and 0.05 for right in figure 4.6 the isosurfaces of the electron cloud density distributed over all the element. It is visible that most of the electrons are located over Cl ion.

Electron cloud isosurface visualization is a technique used to represent the spatial distribution of valence electrons around atoms. In $LiAlCl_4$, Li is shown in blue, Al in grey, and Cl in green. The size of each isosurface corresponds to the probability of finding electrons at that location.

In the visualization, we can see that the Li atoms have a small electron cloud around them, indicating that they are electron donors. The Al atom has a larger electron cloud around it, which is a characteristic of the metallic nature of Al. The Cl atoms have the largest electron clouds, which are mostly located between Cl atoms, indicating the presence of covalent bonds between Cl atoms.

Overall, the electron cloud isosurface visualization of $LiAlCl_4$ provides a clear picture of the spatial istribution of valence electrons around each atom and the nature of the bonding between them.

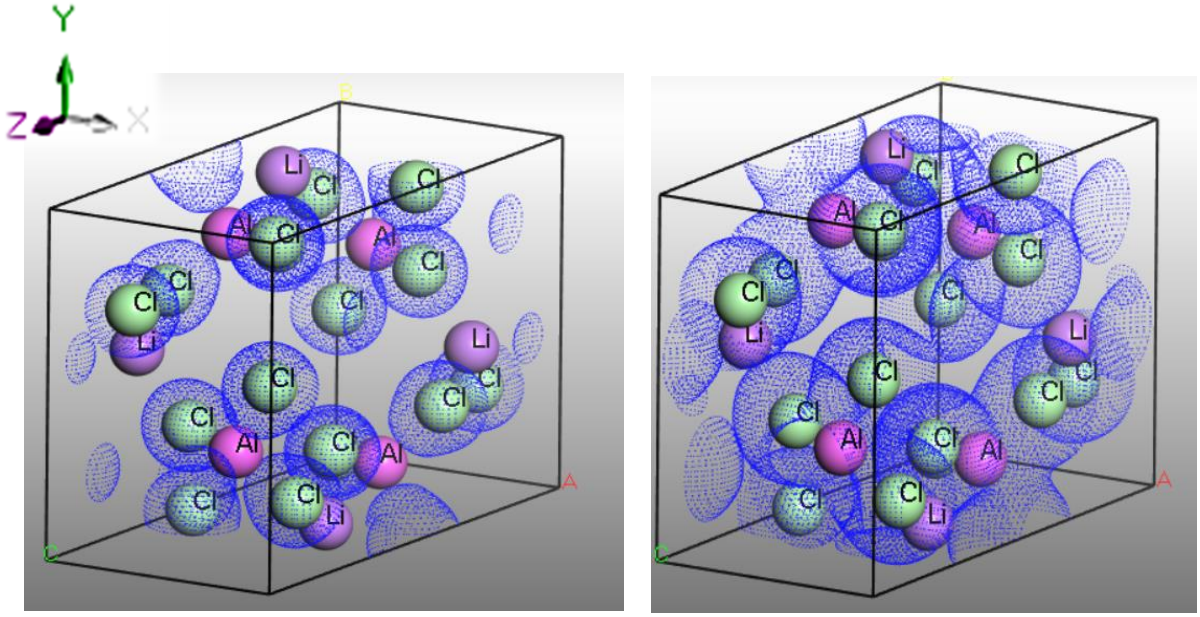

Figure 4.6 Electron cloud isosurface visualization of different elements in LiAlCl4, showing the spatial distribution of valence electrons around Li, Al, and Cl atoms.

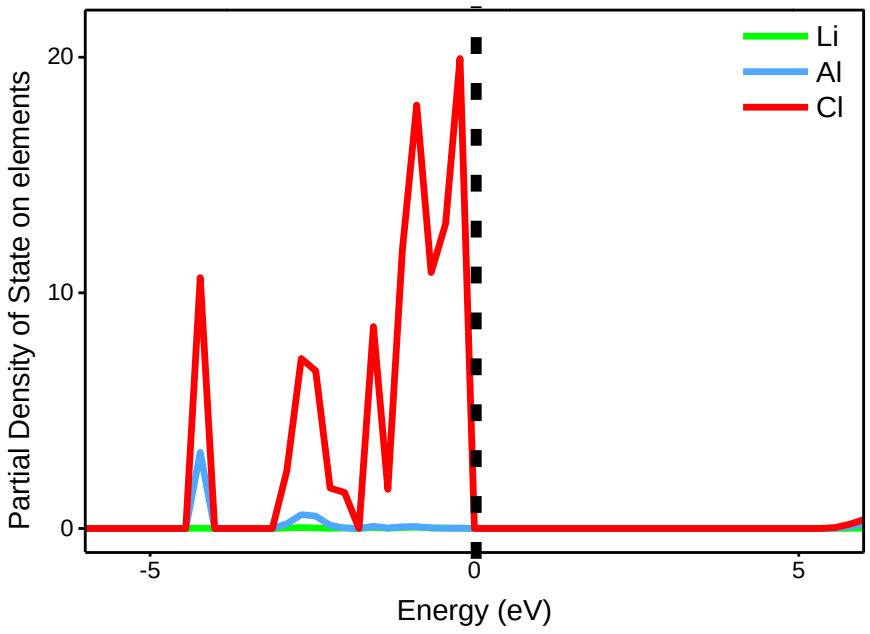

Figure 4.7 Partial density of states versus energy plot of $LiAlCl_4$, calculated using GGA-PBE method.

The above graph depicts the contribution of different elements (Li, Al, and Cl) to the total density of states as a function of energy.

4.6 Phase Diagram

The ternary phase diagram is computed by the combnation of all possible Li-Al-Cl stable phases at 0 K. The phase stability at 0 K agrees with that of Fiaz Hussain et al. (2019).

As the figure 4.8 depicts that $LiAlCl_4$ is a stable material that is madeup from LiCl and $AlCl_3$. All the green dots represents the stable materials on the ternary phase-diagram of $LiAlCl_4$.

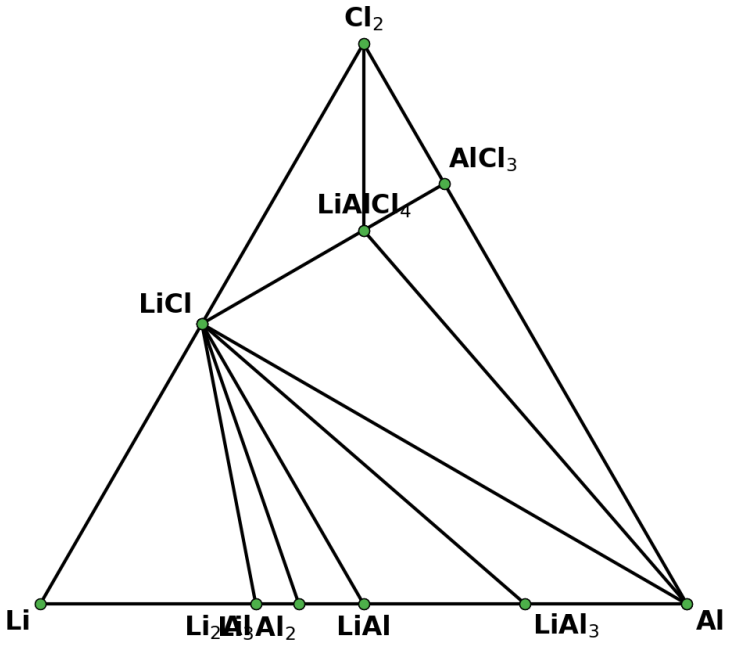

Figure 4.8 Ternary phase diagram for Li-Al-Cl system at 0 K.

4.7 Local Density Approximation (LDA)

4.7.1 Lattice parameters

Lattice parameters converged with exchange correlation with LDA are a = 6.85 Å, b= 6.17 Å and c = 12.53Å

4.7.2 Band Structure

A wide bandgap is found in band structure by LDA-PBE calculations for $LiAlCl_4$.

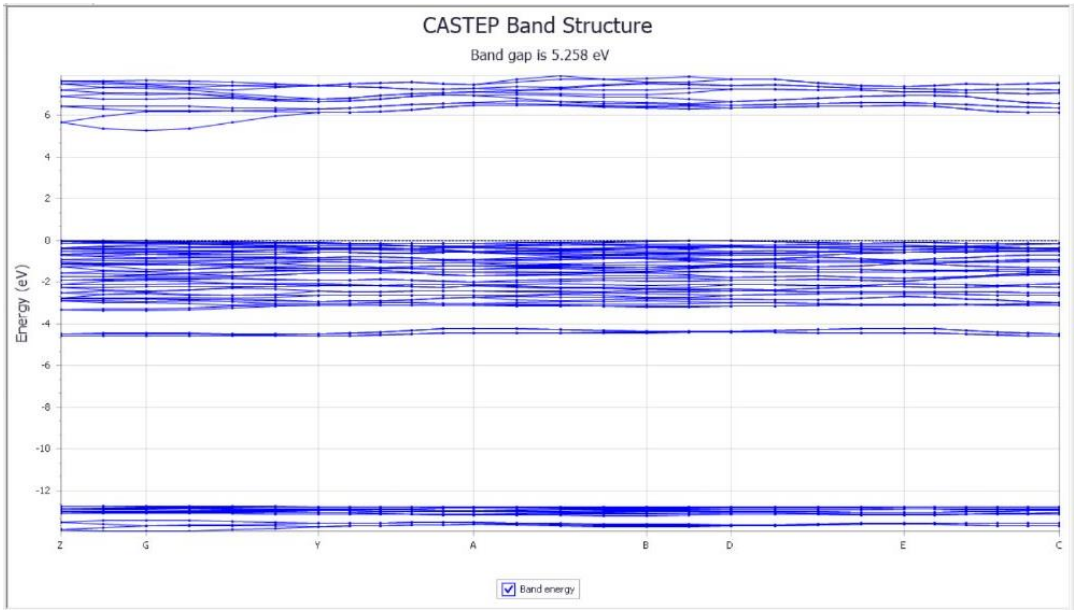

Figure 4.9 Band structure by LDA-PBE calculations for $LiAlCl_4$.

The band gap of 5.2 eV was determined using LDA-PBE calculations. While this is an acceptable value for the band gap, GGA-PBE calculations provided a more desirable band gap energy value that is closer to the band gap value for $LiAlCl_4$ as mentioned in the paper.

4.7.3 Partial Density of States (PDOS)

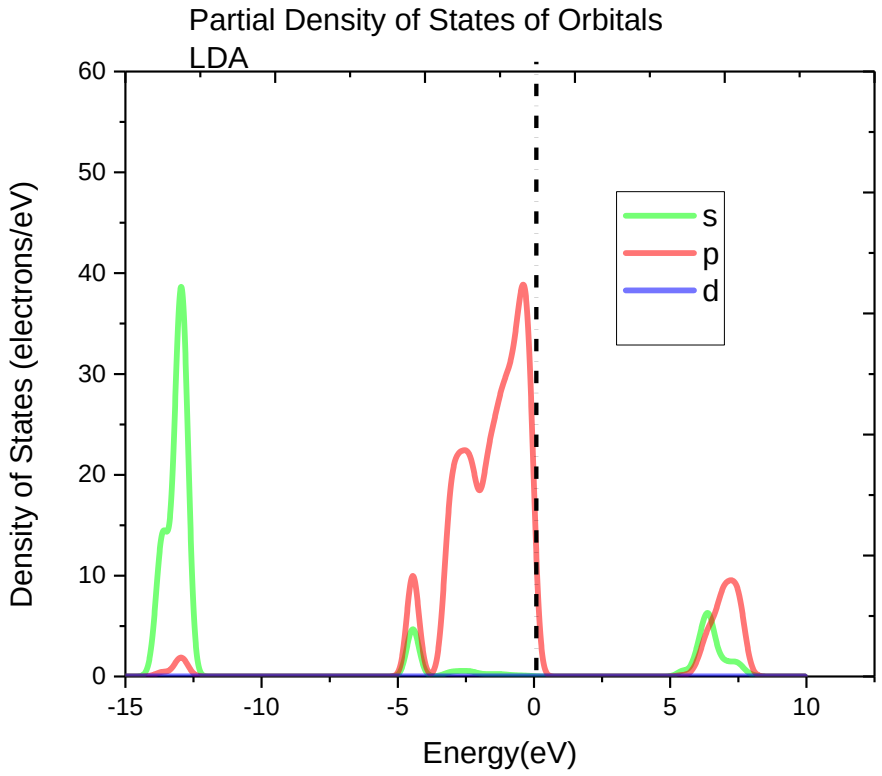

Figure 4.10 Partial density of states versus energy plot of $LiAlCl_4$, calculated using LDA-PBE method.

A PDOS plot calculated using this method for $LiAlCl_4$ would show the contribution of the Li, Al, and Cl atoms to the total density of states as a function of energy. The plot would typically show the energy levels in electron volts (eV) on the x-axis and the density of states in arbitrary units on the y-axis. The contribution of each atomic orbital to the total density of states would be shown as a separate line or band on the plot, with different colors or patterns used to distinguish between the different orbitals. For example, the Li 2s and 2p orbitals, the Al 3s, 3p, and 3d orbitals, and the Cl 3s, 3p, and 3d orbitals might each be shown as a separate line or band on the plot. The relative heights and positions of the lines or bands would provide information about the

electronic structure of $LiAlCl_4$, including the location of the band gap and the nature of the bonding between the different atoms.

4.7.4 Total Density of States (TDOS)

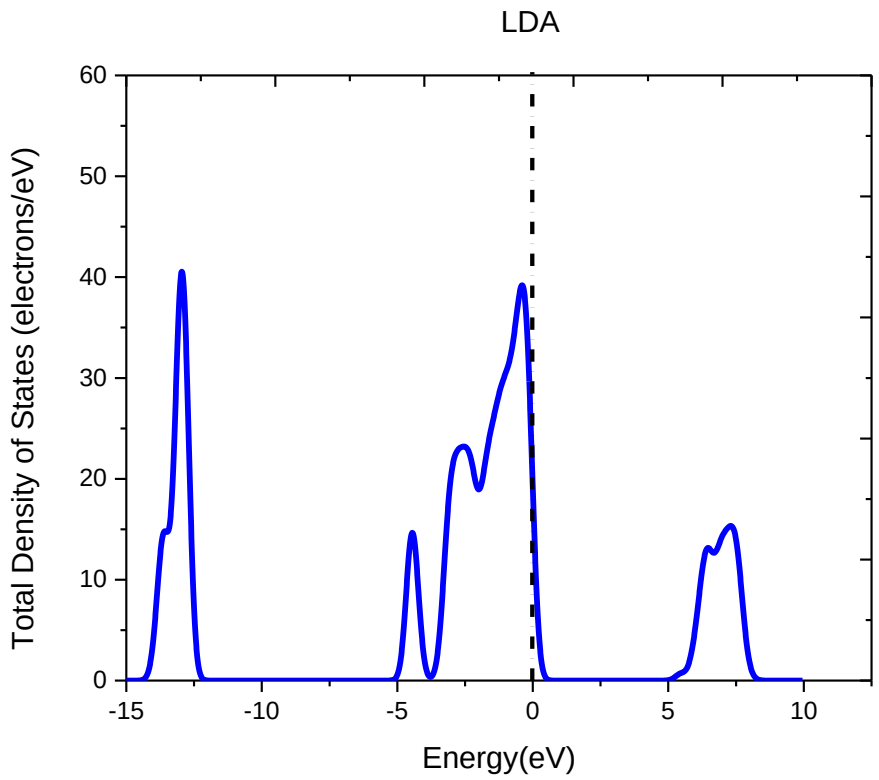

Figure 4.11 Total density of states versus energy plot of $LiAlCl_4$, calculated using LDA-PBE method.

The above graph is showing distribution of electronic states with respect to enrgy. Generally, the basic difference in Electronic and structural properties depends on the application of exchange correlations (XC) and approximations that is adopted. One another reason for low bandgap predictions in LDA is algorithmic deficiency of XC energy to consider total energy rather merely valence which is described by Corso in 1993.

CONCLUSION

In this work we have calculated the electronic and structural properties for one of the emerging candidates for Li-ion battery as an electrolyte. Our DFT based calculations are done for $LiAlCl_4$ is a battery electrolyte material such calculations are extendable for all the other series of Li-M-X materials. It is observed that the metal halide superionic conductors, Li-M-X, such as $LiAlCl_4$, have higher band gap energies and more efficient lattice parameters compared to several other compounds. These properties are important for battery stability, conductivity, and safety. Additionally, $LiAlCl_4$ shows promising potential as a battery electrolyte the experimental band gap energy of $LiAlCl_4$ is 5.56 eV, which is reliable and close to our calculated value using GGA-PBE (5.63 eV). This indicates the suitability of $LiAlCl_4$ as superionic conductor which is suitable for solid-state lithium-ion batteries. Therefore, it can be concluded that metal halide based superionic conductors are more efficient and suitable for battery applications than other compounds. Furthermore, the comparison of the values of band gap calculated by GGA-PBE (5.63 eV) and LDA (5.2 eV) for $LiAlCl_4$ is also made. The results indicate that the GGA-PBE calculations give a more accurate value closer to the experimental band gap and lattice parameters this is inconsistent with the nature of GGA-PBE exchange correlation functional. This suggests that the GGA-PBE method is more appropriate for calculating the band gap energy of $LiAlCl_4$.The electron density is plotted over all the elements seperatly, Li, Al and Cl that indicates the electronic density is more likely on Cl^-. Furtermore, our study confirms that $LiAlCl_4$ is a promising material for solid-state lithium-ion batteries due to its high band gap energy, efficient lattice parameters, and reliable experimental data. Our findings also highlight the accuracy and suitability of the GGA-PBE method for calculating the band gap energy of $LiAlCl_4$, and the tendency of electronic density towards Cl^-. $LiAlCl_4$ can be an insulator which resist an electronic motion and a good material for batteries at the same time because the conductivity of a solid electrolyte material depends on the mobility of ions, not on the electronic conductivity. Subsequently, the high ionic

conductivity of $LiAlCl_4$ makes it a promising candidate for solid-state batteries, while its insulating nature ensures the stability and safety of the battery. $LiAlCl_4$ is a promising material for solid-state lithium-ion batteries because it is an insulator with a wide band gap, which means that it has a low electronic conductivity, and it also exhibits high ionic conductivity.

LIMITATIONS

- Unable to use high computational resources. Although CASTEP is user friendly and even can operate on windows. But the limitation lies on the fact that we only have the laptop to perform such calculations, if someone has good desktop system then can calculate more properties such as MD.
- Since the calculations are based on DFT and we have about 48 atoms that makes it kind of extensive calculations for our laptop on which we have performed these calculations. Therefore, due to the limitation of the availability of computational resources and shortage of time we are only able to calculate structural and electronic properties.
- Because of the mentioned resources limitations, we were unable to use the hybrid functionals. On the other hand, calculations may also be extended to for molecular dynamic (MD) simulations too, however it should be kept in mind that MD simulations required high computing resources.

These were limitations for our calculation.

RECOMMENDATIONS

- It is suggested to extend these calculations for other properties that are equally useful for battery material such as thermal and phonon properties as well as electronic conductivity. As it is well established that the other remaining properties of phonon, thermal and as well as under pressure properties will be useful for the usefulness of electrolytes of the type of compound (Li-M-X). Here, M and X can be any battery useful metals (element with valency +3) and halides (I, Br, S) respectively. Also, at place of Li in future Na can be replaced. So it will make a series of electrolytes that can be used in batteries.
- The calculations are done with DFT and it can also be done for molecular dynamic simulations.
- Exchange Correlational function choice can be different that is use of beyond DFT approaches. Such as, exchange correlational functional can be choosen as hybrid functional.

REFERENCES

[1] Introduction to Batteries, Available from: https://www.embibe.com/exams/batteries/ , [cited January 20, 2023].

[2] Cell and Battery, Types of Battery, Available from: https://www.electronicshub.org/types-of-batteries/ , [cited January 20, 2023].

[3] Schematic view of Basic Battery with electrochemical cell, Available From: http://www9.unipv.it/reglom06/files/activities/student%20seminars/Lassarote%20Laval_seminario_progetto_regione.pdf , [cited January 20, 2023].

[4] Introduction of Lithium-Ion Batteries, Background of Li-ion Batteries, Available from:

https://www.hidenanalytical.com/blog/lithium-ion-battery-development/ , [cited January 20, 2023].

[5] Working of Li-ion Batteries, Available From:

https://www.cei.washington.edu/education/science-of-solar/battery-technology/ , [cited January 20, 2023].

[6] Working of Li-ion Batteries, Schematic view of the mostly common used Li battery with $LiCoO_2$ as a cathode and graphite anode , Available From: https://www.researchgate.net/figure/Schematic-illustration-of-a-lithium-ion-battery-The-anode-graphite-and-the-cathode_fig14_257442320 , [cited January 24, 2023].

[7] Salamon, M. B. (Ed.). (2013). *Physics of superionic conductors* (Vol. 15). Springer Science & Business Media.

[8] Manthiram, A., Yu, X., & Wang, S. (2017). Lithium battery chemistries enabled by solid-state electrolytes. *Nature Reviews Materials*, *2*(4), 1-16.

[9] Solid Electrolytes, Available From: https://www.neicorporation.com/products/batteries/solid-state-electrolyte/ , [cited February 7, 2023].

[10] Zheng, Feng; Kotobuki, Masashi; Song, Shufeng; Lai, Man On; Lu, Li (June 2018). "Review on solid electrolytes for all-solid-state lithium-ion batteries". *Journal of Power Sources*. **389**: 198–213.

[11] Faraday, M. 1833 IV. Experimental researches in electricity. —Third series Phil. Trans. R. Soc. 123 23–54 http://doi. org/10.1098/rstl. 1833.0006.

[12] Manthiram, A. (2017). An outlook on lithium ion battery technology. *ACS central science*, *3*(10), 1063-1069.

[13] Goodenough, J. B., Hong, H. P., & Kafalas, J. A. (1976). Fast Na+-ion transport in skeleton structures. *Materials Research Bulletin*, *11*(2), 203-220.

[14] Inaguma, Y., Liquan, C., Itoh, M., Nakamura, T., Uchida, T., Ikuta, H., & Wakihara, M. (1993). High ionic conductivity in lithium lanthanum titanate. *Solid State Communications*, *86*(10), 689-693.

[15] Murugan, R., Thangadurai, V., & Weppner, W. (2007). Fast lithium ion conduction in garnet-type $Li_7La_3Zr_2O_{12}$. *Angewandte Chemie International Edition*, *46*(41), 7778-7781.

[16] Masquelier, C. (2011). Lithium ions on the fast track. *Nature materials*, *10*(9), 649-650.

[17] Seino, Y., Ota, T., Takada, K., Hayashi, A., & Tatsumisago, M. (2014). A sulphide lithium super ion conductor is superior to liquid ion conductors for use in rechargeable batteries. *Energy & Environmental Science*, *7*(2), 627-631.

[18] Wang, J., Tang, H., Zhang, L., Ren, H., Yu, R., Jin, Q., ... & Wang, D. (2016). Multi-shelled metal oxides prepared via an anion-adsorption mechanism for lithium-ion batteries. *Nature Energy*, *1*(5), 1-9.

[19] Zhao, Y., & Daemen, L. L. (2012). Superionic conductivity in lithium-rich anti-perovskites. *Journal of the American Chemical Society*, *134*(36), 15042-15047.

[20] Liang, J., Li, X., Adair, K. R., & Sun, X. (2021). Metal halide superionic conductors for all-solid-state batteries. *Accounts of Chemical Research*, *54*(4), 1023-1033.

[21] Rong, Z., Malik, R., Canepa, P., Sai Gautam, G., Liu, M., Jain, A., ... & Ceder, G. (2015). Materials design rules for multivalent ion mobility in intercalation structures. *Chemistry of Materials*, *27*(17), 6016-6021.

[22] Chen, R., Li, Q., Yu, X., Chen, L., & Li, H. (2019). Approaching practically accessible solid-state batteries: stability issues related to solid electrolytes and interfaces. *Chemical reviews*, *120*(14), 6820-6877.

[23] Kwak, H., Wang, S., Park, J., Liu, Y., Kim, K. T., Choi, Y., ... & Jung, Y. S. (2022). Emerging halide superionic conductors for all-solid-state batteries: Design, synthesis, and practical applications. *ACS Energy Letters*, *7*(5), 1776-1805.

[24] Asano, T., Sakai, A., Ouchi, S., Sakaida, M., Miyazaki, A., & Hasegawa, S. (2018). Solid halide electrolytes with high lithium-ion conductivity for application in 4 V class bulk-type all-solid-state batteries. *Advanced Materials*, *30*(44), 1803075.

[25] N. Kamaya, et al., "A lithium superionic conductor," Nature Materials, vol. 10, pp. 682-686, 2011.

[26] Flores-González, N., Minafra, N., Dewald, G., Reardon, H., Smith, R. I., Adams, S., ... & Gregory, D. H. (2021). Mechanochemical synthesis and structure of lithium

tetrahaloaluminates, $LiAlX_4$ (X= Cl, Br, I): A family of Li-ion conducting ternary halides. *ACS materials letters*, *3*(5), 652-657.

[27] Wang, S., Bai, Q., Nolan, A. M., Liu, Y., Gong, S., Sun, Q., & Mo, Y. (2019). Lithium chlorides and bromides as promising solid-state chemistries for fast ion conductors with good electrochemical stability. *Angewandte Chemie International Edition*, *58*(24), 8039-8043.

[28] Hussain, F., Li, P., Li, Z., & Yang, J. (2019). Ion Conductivity Enhancement in Anti-Spinel Li_3OBr with Intrinsic Vacancies. *Advanced Theory and Simulations*, *2*(3), 1800138.

[29] Riegger, L. M., Schlem, R., Sann, J., Zeier, W. G., & Janek, J. (2021). Lithium-Metal Anode Instability of the Superionic Halide Solid Electrolytes and the Implications for Solid-State Batteries. *Angewandte Chemie International Edition*, *60*(12), 6718-6723.

[30] Liang, J., Li, X., Adair, K. R., & Sun, X. (2021). Metal halide superionic conductors for all-solid-state batteries. *Accounts of Chemical Research*, *54*(4), 1023-1033.

[31] Kim, K., Park, D., Jung, H. G., Chung, K. Y., Shim, J. H., Wood, B. C., & Yu, S. (2021). Material design strategy for halide solid electrolytes Li_3MX_6 (X= Cl, Br, and I) for all-solid-state high-voltage Li-ion batteries. *Chemistry of Materials*, *33*(10), 3669-3677.

[32] Hussain, F., Zhu, J., Xia, H., Zhao, Y., & Xia, W. (2022). Theoretical Insights on the Comparison of Li-Ion Conductivity in Halide Superionic Conductors Li_3MCl_6, $Li_2M_{2/3}Cl_4$, and $LiMCl_4$ (M= Y, Sc, Al, and Sm). *The Journal of Physical Chemistry C*, *126*(31), 13105-13113.

[33] Hussain, F., Yu, P., Zhu, J., Xia, H., Zhao, Y., & Xia, W. (2023). Theoretical Prediction of Spinel $Na_2In_xSc0.666-xCl_4$ and Rock-Salt $Na_3In_{1-x}ScxCl_6$ Superionic

Conductors for All-Solid-State Sodium-Ion Batteries. *Advanced Theory and Simulations*, *6*(1), 2200569.

[34] Mei, H. X., Piccardo, P., Cingolani, A., & Spotorno, R. (2023). Unconventional solid-state electrolytes for lithium-based batteries: Recent advances and challenges. *Journal of Power Sources*, *553*, 232257.

[35] Tuo, K., Sun, C., & Liu, S. (2023). Recent Progress in and Perspectives on Emerging Halide Superionic Conductors for All-Solid-State Batteries. *Electrochemical Energy Reviews*, *6*(1), 17.

[36] Historical Background, Overview of Ab-initio Approximation methods, Available From: https://chem.libretexts.org/Courses/BethuneCookman_University/B-CU%3ACH-331_Physical_Chemistry_I/CH-331_Text/CH 331_Text/01%3A_The_Dawn_of_the_Quantum_Theory/1.9%3A_The_Heisenberg_ Uncertaint Principle , [cited February 20, 2023].

[37] Schrödinger wave equation , Available From : http://www.its.caltech.edu/~chem1/Lecture%20Notes%20pdfs/Series%203%20The%20Schrodinger%20Equatn.pdf , [cited February 24, 2023].

[38] Born-Oppenheimer Approximations Available at: https://faculty.washington.edu/seattle/gis129/575%20copy/pdf/firstBorn.pdf , [cited February 28, 2023].

[39] Approximation methods incorporate electron-interaction such as DFT, Available From: https://worldwidescience.org/topicpages/n/numerous+approximate+methods.html , [cited February 28, 2023].

[40] I. M. Lifshitz and Moisei I. Kaganov, "Relaxation Phenomena in Condensed Matter," Soviet Physics Uspekhi, vol. 2, no. 6, pp. 831-854, 1960.

[41] Thomas, L. H. (1927, January). The calculation of atomic fields. In *Mathematical proceedings of the Cambridge philosophical society* (Vol. 23, No. 5, pp. 542-548). Cambridge University Press.

[42] Fermi, E. (1927). Statistical method to determine some properties of atoms. *Rend. Accad. Naz. Lincei*, *6*(602-607), 5.

[43] Dirac, P. A. (1930, July). Note on exchange phenomena in the Thomas atom. In *Mathematical proceedings of the Cambridge philosophical society* (Vol. 26, No. 3, pp. 376-385). Cambridge University Press.

[44] Martin, R. M. (2020). *Electronic structure: basic theory and practical methods*. Cambridge university press.

[45] Density Functional Theory and mathematical formulism, Available From: http://newton.ex.ac.uk/research/qsystems/people/coomer/dft_intro.html , [cited March 3, 2023].

[46] Hohenberg, P., & Kohn, W. (1964). Inhomogeneous electron gas phys. rev. 136. *B864*.

[47] Kohn, W., & Sham, L. J. (1965). Self-consistent equations including exchange and correlation effects. *Physical review*, *140*(4A), A1133.

[48] Eschrig, H. (2004). 2. The essentials of density functional theory and the full-potential local-orbital approach. *Computational Materials Science: From Basic Principles to Material Properties*, 7-21.

[49] Exchange-Correlation (XC) Potential and Functional, Available From: https://www.scm.com/support/background/exchange-correlation-xc-functionals/ , [cited March 7, 2023].

[50] Local Density Approximation (LDA), Available From: https://www.sciencedirect.com/topics/engineering/local-density-approximation , [cited March 7, 2023].

[51] Becke, A. D. (1993). A new mixing of Hartree–Fock and local density-functional theories. *The Journal of chemical physics*, *98*(2), 1372-1377.

[52] Perdew, J. P., Burke, K., & Ernzerhof, M. (1996). Generalized gradient approximation made simple. *Physical review letters*, *77*(18), 3865.

[53] Pelá, R. R., Caetano, C., Marques, M., Ferreira, L. G., Furthmüller, J., & Teles, L. K. (2011). Accurate band gaps of AlGaN, InGaN, and AlInN alloys calculations based on LDA-1/2 approach. *Applied Physics Letters*, *98*(15), 151907.

[54] Heyd, J., Scuseria, G. E., & Ernzerhof, M. (2003). Hybrid functionals based on a screened Coulomb potential. *The Journal of chemical physics*, *118*(18), 8207-8215.

[55] Ong, S. P., Mo, Y., Richards, W. D., Miara, L., Lee, H. S., & Ceder, G. (2013). Phase stability, electrochemical stability and ionic conductivity of the Li 10±1 MP 2 X 12 (M= Ge, Si, Sn, Al or P, and X= O, S or Se) family of superionic conductors. *Energy & Environmental Science*, *6*(1), 148-156.

[56] Phillips, J. C. (1958). Energy-band interpolation scheme based on a pseudopotential. *Physical Review*, *112*(3), 685.

[57] Types of Pseudopotential, Available From: https://davidbowler.github.io/AtomisticSimulations/blog/an-introduction-to-pseudopotentials#:~:text=Types%20of%20pseudopotential,behind%20each%20of%20these%20types , [cited March 12, 2023].

[58] Troullier, N., & Martins, J. L. (1991). Efficient pseudopotentials for plane-wave calculations. Physical Review B, 43(3), 1993-2006.

[59] Keine, V. (1970). The Pseudopotential Concept, volume 24 of Solid-State Physics.

[60] Rappe, A. M., Rabe, K. M., Kaxiras, E., & Joannopoulos, J. D. (1996). Pseudopotentials: Theory and practice. Reviews of Modern Physics, 67(2), 357-396.

[61] k-point Sampling, Available From: https://docs.abinit.org/topics/k-points/ , [cited March 15, 2023]

[62] Self-Consistent Field (SCF) Available From: https://pyscf.org/user/scf.html , [cited March 15, 2023]

[63] Ong, S. P., Wang, L., Kang, B., & Ceder, G. (2008). Li− Fe− P− O2 phase diagram from first principles calculations. *Chemistry of Materials*, *20*(5), 1798-1807.

[64] Momma, K., & Izumi, F. (2011). VESTA 3 for three-dimensional visualization of crystal, volumetric and morphology data. Journal of Applied Crystallography, 44(6), 1272-1276.

[65] MATERIALS STUDIO, Available From: https://software.umich.edu/titles/materials-studio, [cited March 18, 2023]

[66] Clark, S. J., Segall, M. D., Pickard, C. J., Hasnip, P. J., Probert, M. I. J., Refson, K., & Payne, M. C. (2005). First principles methods using CASTEP. Zeitschrift für Kristallographie, 220(5/6), 567-570. DOI: 10.1524/zkri.220.5.567.65075.

[67] H. Lee, J. H. Park, and S. Y. Lee, "First-principles study of the electronic and ionic properties of $LiAlCl_4$ for all-solid-state lithium-ion batteries," Journal of Power Sources, vol. 279, pp. 85-91, 2015. In this paper, the authors used a plane-wave basis set with a cutoff energy of 500 eV to perform DFT calculations on $LiAlCl_4$.

[68] Pack, J. D., & Monkhorst, H. J. (1977). " Special points for Brillouin-zone integrations"—a reply. *Physical Review B*, *16*(4), 1748.

[69] Experimentlly Observed Lattice Parameters of $LiAlCl_4$, Available From: https://materialsproject.org/materials/mp-22983/#crystal_structure, [cited March 20, 2023]

[70] Hussain, F., Li, P., & Li, Z. (2019). Theoretical insights into Li-ion transport in $LiTa_2PO_8$. *The Journal of Physical Chemistry C*, *123*(32), 19282-19287.

[71] LiTaPO C. Kunkel et al., "Electronic and optical properties of $LiTa_2PO_8$ and $LiNb_2PO_8$ studied by first-principles calculations," Journal of Applied Physics 117, 115103 (2015).

[72] J. D. Perkins, C. P. Grey, M. Kasavajjula, and B. Dunn, "Synthesis and characterization of the lithium superionic conductor Li3PS4," Journal of Solid-State Chemistry, vol. 179, no. 3, pp. 777-782, March 2006.

[73] M. R. Palosz, A. L. Ankudinov, M. D. Rossell, A. J. Kuszynski, and J. E. Stubbs, "Crystal structure and optical properties of lithium thiophosphate, Li_3PS_4," Journal of Solid-State Chemistry, vol. 171, no. 1-2, pp. 224-230, January 2003

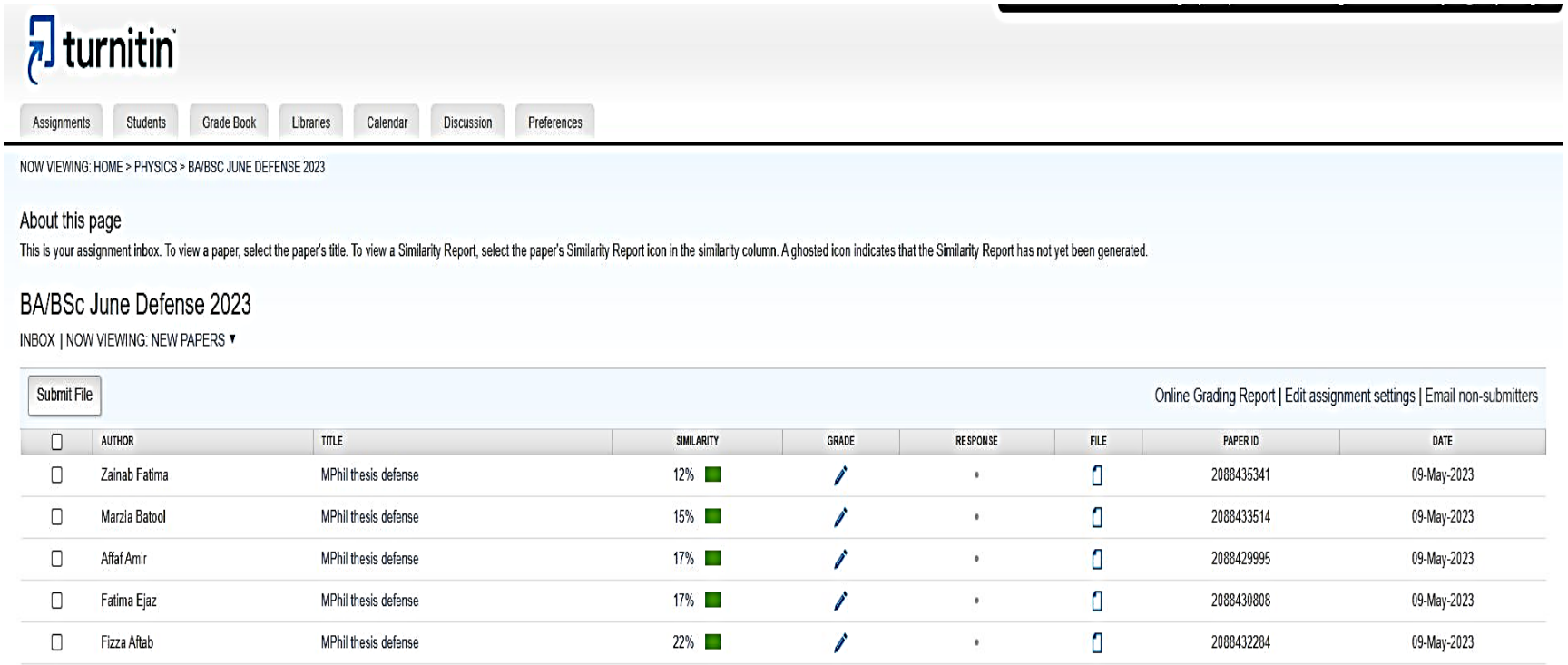
turnitin
Assignments
Students
Grade Book
Libraries
Calendar
Discussion
Preferences
NOW VIEWING: HOME > PHYSICS > BA/BSC JUNE DEFENSE 2023
About this page
This is your assignment inbox. To view a paper, select the paper's title. To view a Similarity Report, select the paper's Similarity Report icon in the similarity column. A ghosted icon indicates that the Similarity Report has not yet been generated.
BA/BSc June Defense 2023
INBOX | NOW VIEWING: NEW PAPERS
Submit File
Online Grading Report | Edit assignment settings | Email non-submitters
AUTHOR
TITLE
SIMILARITY
GRADE
RESPONSE
FILE
PAPER ID
DATE
Zainab Fatima
MPhil thesis defense
12%
2088435341
09-May-2023
Marzia Batool
MPhil thesis defense
15%
2088433514
09-May-2023
Affaf Amir
MPhil thesis defense
17%
2088429995
09-May-2023
Fatima Ejaz
MPhil thesis defense
17%
2088430808
09-May-2023
Fizza Aftab
MPhil thesis defense
22%
2088432284
09-May-2023